A Family of Singly Periodic Minimal Surfaces Invariant under a Screw Motion

Michael Callahan, David Hoffman and Hermann Karcher

CONTENTS

Callahan was partially supported by the Rhodes Trust.

Hoffman was supported by research grant DEFG02-86ER25015 of the Applied Mathematical Science subprogram of the Office of Energy Research of the US Department of Energy, and by research grants DMS-9011083 and DMS-9101903 of the Division of Mathematical Sciences of the National Science Foundation.

Karcher was partially supported by Sonderforschungsbereich SFB256 at Bonn.

We construct explicitly, using the generalized Weierstrass representation, a complete embedded minimal surface $M_{k,\theta}$ invariant under a rotation of order $k+1$ and a screw motion of angle 2θ about the same axis, where $k>0$ is any integer and θ is any angle with $|\theta|<\pi/(k+1)$. The existence of such surfaces was proved in [Callahan et al. 1990], but no practical procedure for constructing them was given there.

We also show that the same problem for $\theta=\pm\pi/(k+1)$ does not have a solution enjoying reflective symmetry; the question of the existence of a solution without such symmetry is left open.

INTRODUCTION

In [Callahan et al. 1989], two of the authors and W. Meeks found examples of translation-invariant, embedded minimal surfaces with an infinite number of topological ends. For each $k>0$, a surface M_k was constructed that is invariant with respect to a translation parallel to the x_3-axis and under a rotation of order $k+1$ around the x_3-axis.

The method of construction was generalized in [Callahan et al. 1990] to obtain the first known examples of embedded singly periodic minimal surfaces with an infinite number of topological ends and invariant under screw motions (with a nontrivial rotational component). For each integer $k>0$ and each angle θ with $|\theta|<\pi/(k+1)$, there exists an embedded surface $M_{k,\theta}$ whose orientation-preserving symmetry group contains a rotation of order $k+1$ around the x_3-axis and a screw motion—a unit translation in the x_3-direction, followed by a 2θ rotation around it. Examples of such surfaces,

1058-6458/93 $0.50 per page

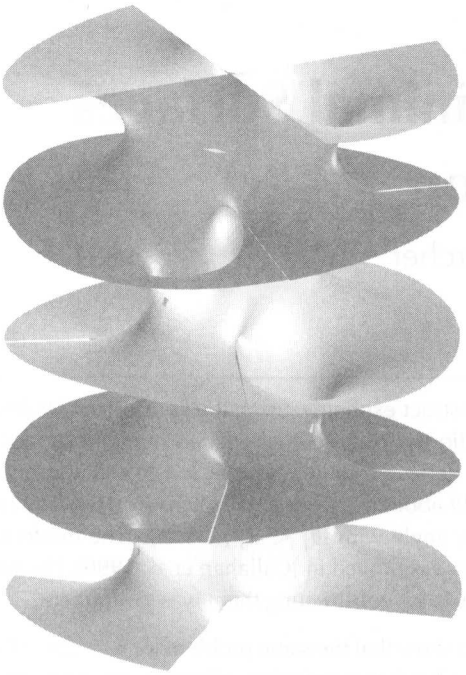

$\theta = 10.5°$

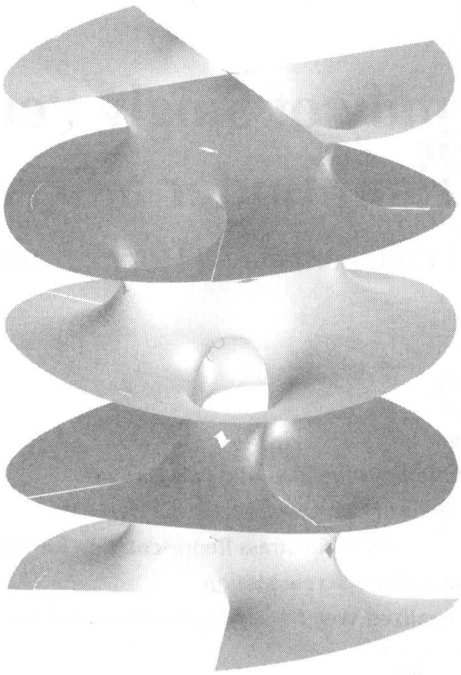

$\theta = 30°$

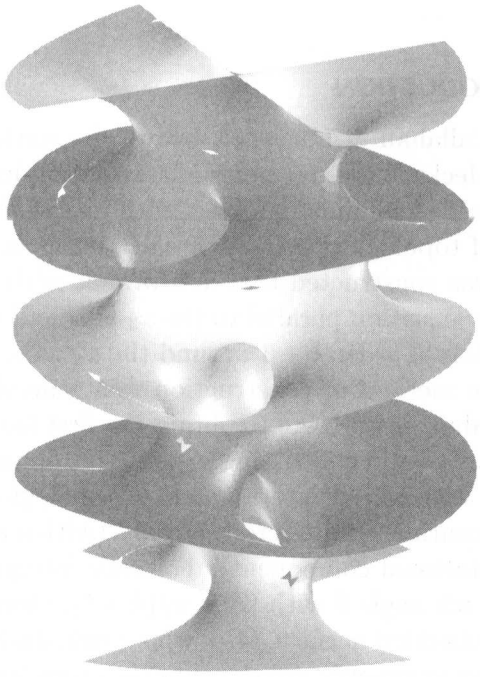

$\theta = 40°$

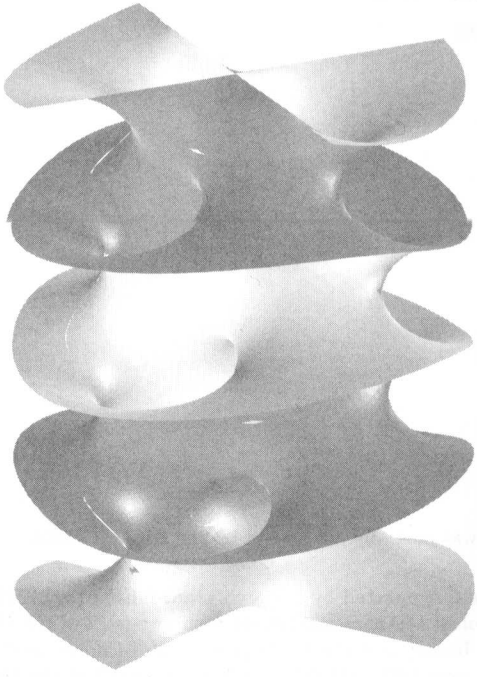

$\theta = 60°$

FIGURE 1. Surfaces $M_{k,\theta}$ for $k = 1$ and increasing values of θ (approximate). See also Section 5, especially Figure 11.

constructed using the techniques described in the present article, are shown in Figure 1.

Although the surfaces $M_{k,\theta}$ were conceived as smooth deformations of the singly periodic examples M_k, the proof in [Callahan et al. 1990] did not construct these deformations. In fact, it left open the following questions:

1. Do the $M_{k,\theta}$ depend smoothly on θ? If so, are they deformations of M_k?
2. Are the surfaces $M_{k,\theta}$ unique?
3. Is there a surface $M_{k,\pi/(k+1)}$? To be more precise: the symmetry groups of the $M_{k,\theta}$ have a single limit as $\theta \to \pm\pi/(k+1)$. This limit group contains a translation but is different from the symmetries of $M_{k,0}$. Is there a surface with this symmetry group and obvious properties generalizing the $M_{k,\theta}$?

A more down-to-earth question concerned the appearance of these surfaces. The existence proof in [Callahan et al. 1990] used a minimax argument involving unstable minimal annuli spanning a fixed boundary. This technique provided no procedure for producing a fair numerical approximation (see Section 2.1). In [Callahan et al. 1989], the conjugate surface method was used to construct the translation-invariant examples M_k (see Section 2.2). This technique, however, requires reflective symmetries, which the surfaces $M_{k,\theta}$ do not possess in general. Among the methods currently in use, only the Weierstrass representation is left. This paper explains, among other things, how we were able to make pictures such as those shown in Figure 1.

The use of this method in computations that support and guide theoretical investigations in the study of embedded minimal surfaces is well documented [Callahan et al. 1988; Hoffman 1987a,b; Hoffman and Karcher; Hoffman and Meeks 1985a, 1985b, 1987, 1990; Karcher 1988, 1989b; Wohlgemuth 1991]. However, for the surfaces $M_{k,\theta}$, we were faced with a computational problem of greater difficulty, for two reasons. First, while the Gauss map g of a translation-invariant minimal surface descends to a meromorphic function on the quotient surface, the quotient by a screw motion only allows dg/g to descend. To produce a Gauss map on the quotient, suitable for integration in a generalized Weierstrass representation, one has to integrate the form

$$\mu := \frac{dg}{g}$$

and then use the multivalued function $\tilde{g} = \exp \int \mu$. This adds another level of complexity to the computational problem, and makes the associated period problem more difficult. Secondly, even though the generalized Weierstrass representation has been known for some years [Karcher 1988; Meeks and Rosenberg 1994], it has not been used frequently to compute examples. It was not clear, a priori, that everything would work; complications and obstacles could arise that would require significant modification of our computational techniques.

One of our goals was to expand our computational techniques to include regular use of the generalized Weierstrass representation of the surfaces $M_{k,\theta}$. There are other situations in which the existence of surfaces with very few symmetries is not known; this representation, coupled with numerical searches and exploratory graphics, could contribute a great deal to theoretical understanding. The current situation seemed like a good first test case for our experimental methods because we had very simple, regular end behavior (all ends are planar) and we had an existence proof in hand. Thus we were not likely to encounter unexpected theoretical difficulties, and, assuming we did, we were likely to actually find some examples. Of course we would also get computer-generated images of the surfaces themselves. In this paper, we describe these computations and present some of the calculated images of the surfaces $M_{k,\theta}$.

We conclude this introduction with an outline of the paper. In Section 1, we give a quick survey of the known singly periodic embedded minimal surfaces. In Section 2, we discuss the techniques used in their construction. Section 3 is devoted to the

generalized Weierstrass representation for minimal surfaces invariant under a screw motion and having only planar ends. In Section 4 we derive the representation for the surfaces $M_{k,\theta}$. The numerical computations are described in Section 5.

In regard to question 1, our work confirms beyond reasonable doubt that there is a smooth family of embedded, singly periodic minimal surfaces that deform the surface M_k and are invariant under a screw motion. (We have not carried out the details of a degree-theory proof showing that the period problem can be solved.)

In regard to question 2, the numerical evidence suggests that there is only one surface for each θ and that, in fact, the parameters describing the surfaces are monotonic in θ. We note that, although embeddedness of the surfaces $M_{k,\theta}$ comes free with the minimax method of [Callahan et al. 1990], we do not know a priori that the surfaces computed here are the same ones, and so we must also prove embeddedness. A continuity argument from [Hoffman et al.] can be used to do this. (In any case the figures leave virtually no doubt.)

Question 3 is considered in Section 6. Here we must report that we were initially misled by numerical results and computer graphics. For values of θ very near to $\pm\pi/(k+1)$, we were able to solve the period problem numerically. This seemed to give evidence for the existence of $M_{k,\pi/(k+1)}$. The computed $M_{k,\pi/(k+1)}$ appeared to have vertical planes of symmetry. If one *assumes* the existence of such symmetries, there is a much simpler parametrization using the traditional Weierstrass representation (that is, one where g is well-defined on the quotient). The period problem here is one-dimensional, with one free parameter, and the period is much easier to compute. The computations suggested that the period did *not* change sign, but did approach zero asymptotically for large values of the parameter. In fact, it turns out that we can prove that the period problem is *not* solvable. We do this in Section 6. The question of the existence of a surface $M_{k,\pi/(k+1)}$ without reflective symmetry is still open.

1. SINGLY PERIODIC EMBEDDED MINIMAL SURFACES

1.1. The Three Types

Singly periodic embedded minimal surfaces S in $\mathbf{R}^3$ are naturally classified by their behavior at infinity, that is, by their number of topological ends. There are three possibilities: one, two, or infinitely many ends.

A typical example with one topological end is Scherk's singly periodic surface, which is invariant under a translation (Figure 2). Another, even older, example with one topological end is the helicoid, which is invariant under a one-parameter group of screw motions. (To see that these surfaces have one end, just observe that the portion of the complete surface not drawn is connected; this is true for the complement of any compact portion of the surface.) This class of single-ended, singly periodic, properly embedded minimal surfaces has been studied a great deal recently and many new examples have been found [Hoffman et al. 1993, 1994; Karcher 1988, 1989a; Meeks and Rosenberg 1994]. For every such example, there is a translation or a screw motion that leaves the surface invariant and that generates a subgroup of finite index in the total symmetry group of the surface. (Here we explicitly exclude embedded doubly periodic surfaces, which are invariant under a lattice of translations.)

There is but one embedded minimal surface with two topological ends that is invariant under an infinite symmetry group: the catenoid [Schoen 1983]. It is well known that the catenoid is the only nonplanar minimal surface of rotation (see, for example, [do Carmo 1976; Hoffman and Meeks 1990; Osserman 1986]).

The third class, the one that will concern us here, is the class of properly embedded, singly periodic minimal surfaces having more than two ends (or, if you like, having more than one end and distinct from the catenoid). The basic appearance of such surfaces is governed by the following structure theorem:

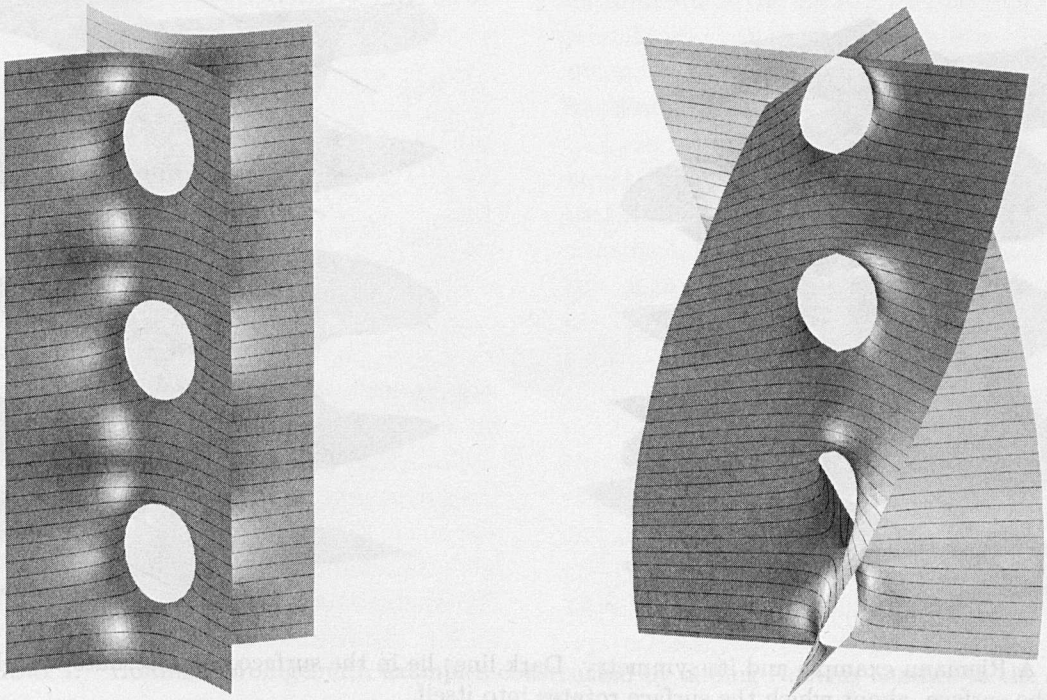

FIGURE 2. Scherk's singly periodic surface, which has one topological end, and a twisted deformation found by Karcher and Pitts.

Theorem 1.1 [Callahan et al. 1990]. *Suppose S is a properly embedded minimal surface in $\mathbf{R}^3$ with an infinite symmetry group and more than one topological end. Then, if S is not the catenoid:*

(a) *The symmetry group of S contains an infinite cyclic subgroup of finite index, generated by a screw motion s.*

(b) *M has an infinite number of ends. Any end that is topologically annular is planar, that is, asymptotic to the exterior of a compact set in a flat plane. If the screw motion s has nontrivial rotational part, the translation is orthogonal to the planar ends.*

(c) *The quotient $\Sigma = S/s$ has finite total curvature if and only if Σ has finite topology, in which case Σ is conformally a compact Riemann surface $\bar{\Sigma}$ punctured at a finite number r of points, and the total curvature is*

$$\int_{\Sigma} K\, dA = 2\pi(\chi(\Sigma) - r).$$

1.2. Riemann's Examples

The classical examples of surfaces satisfying the conditions of Theorem 1.1, and for many years the only ones known, were the surfaces $\mathcal{R}$ of Riemann (Figure 3), which form a one-parameter family. Each $\mathcal{R}$ is fibered by round circles: its intersection with any plane parallel to a planar end is a round circle, the only exception being those planes actually asymptotic to the ends, which intersect $\mathcal{R}$ in straight lines. All these lines are parallel and lie in a single plane P. The surfaces possess a single vertical plane of symmetry V. The subgroup of the symmetry group consisting of orientation-preserving translations is generated by a vector t in the direction of $P \cap V$, whose length is twice the distance between successive lines on $\mathcal{R}$. (Translation by $\frac{1}{2}t$ reverses the orientation of the surface.)

By the Schwarz reflection principle, a minimal surface that contains a line is symmetric under 180° rotation about that line. Rotation about two

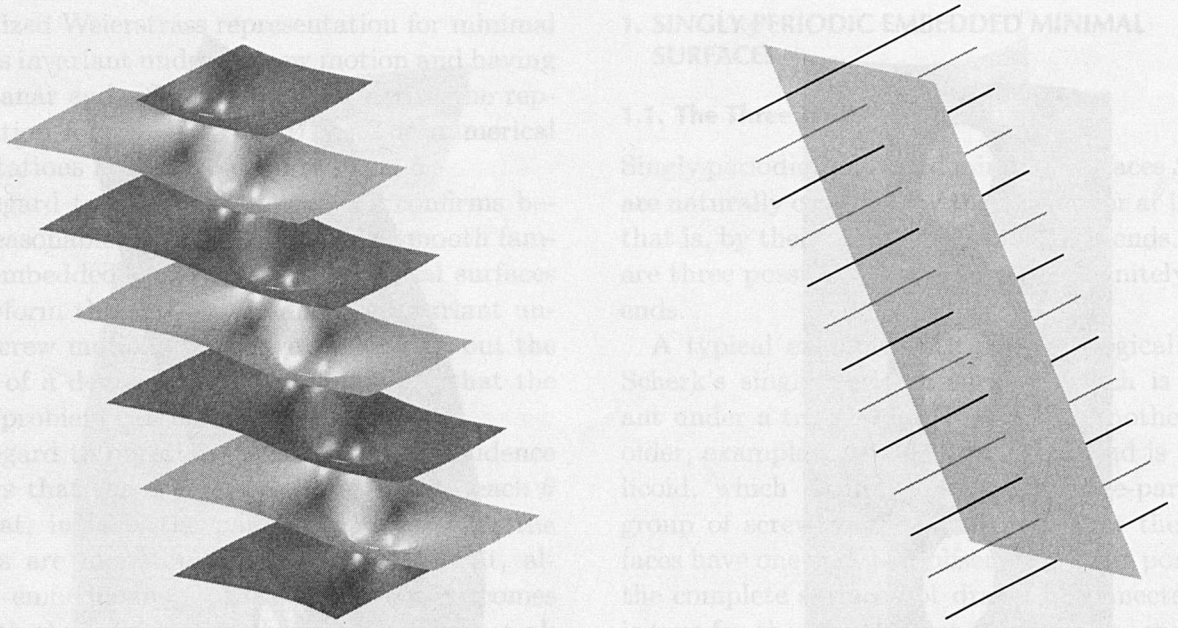

FIGURE 3. A Riemann example and its symmetry. Dark lines lie in the surface and alternate with light lines, normal to the surface, about which the surface rotates into itself.

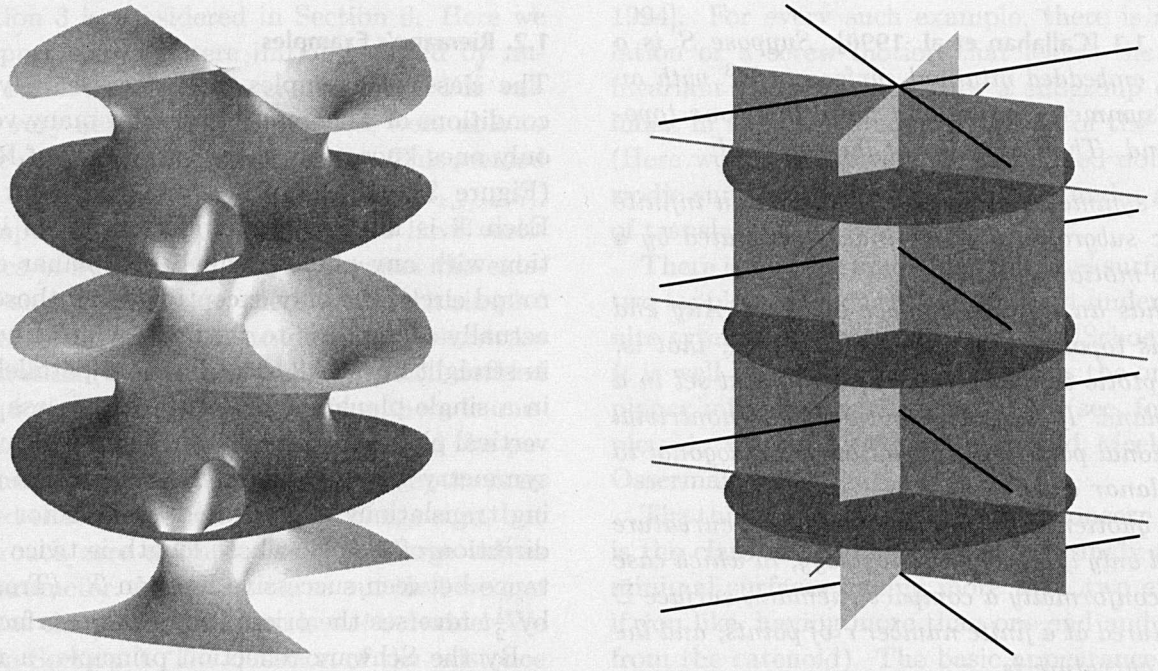

FIGURE 4. The surface M_1 and its symmetry lines and planes.

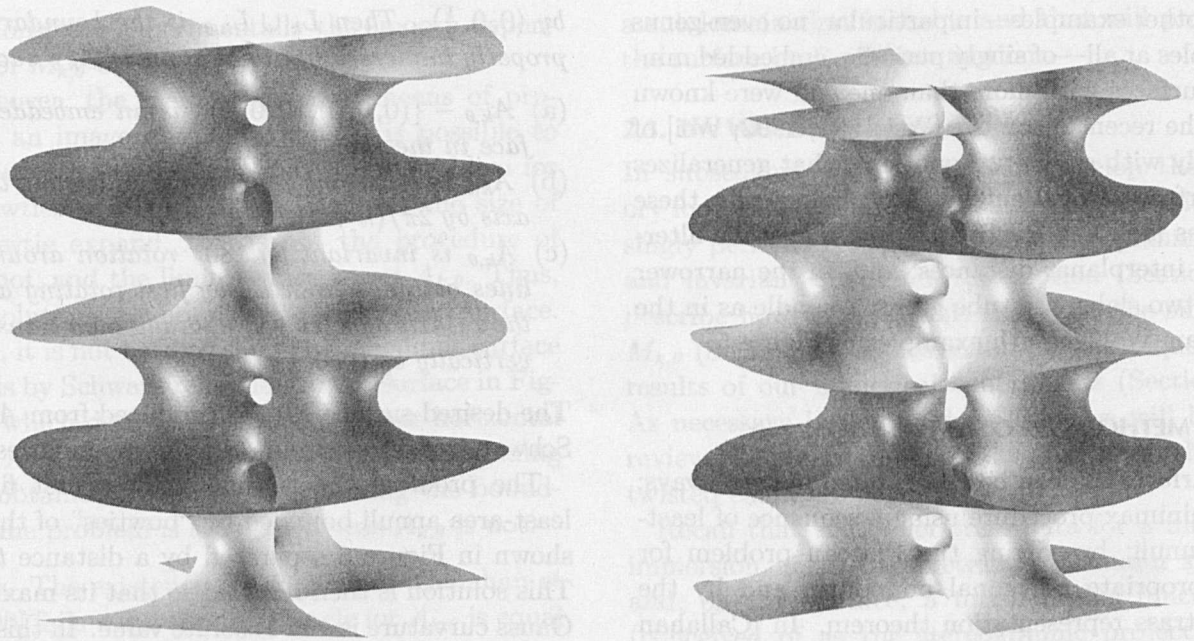

FIGURE 5. Hoffman–Wohlgemuth examples constructed by adding Neovius handles to the M_k.

successive lines generates t. Together with reflection in V, this gives all the evident symmetries of $\mathcal{R}$. However, there is one additional type of symmetry. The lines in P parallel to the lines in $P \cap \mathcal{R}$ and halfway between them meet $\mathcal{R}$ orthogonally, and 180° rotation about these *normal symmetry lines* is a symmetry of $\mathcal{R}$.

The quotient of $\mathcal{R}$ by the translation t is a genus-one surface with two ends. By Theorem 1.1(c), $\mathcal{R}/t$ must be, conformally, a torus punctured in two points. Because of all its inherited reflective symmetry, it is a rectangular torus.

1.3. Modern Translation-Invariant Examples

For over one hundred years, Riemann's examples were the only ones known. Recently [Callahan et al. 1989], an infinite sequence M_k of new examples was constructed (Figure 4), each of which, after normalization, is invariant under a vertical translation t of length 1. They share the following additional properties:

(a) Each M_k has flat ends asymptotic to horizontal planes at integral and half-integral heights.

(b) Horizontal planes intersect M_k in closed Jordan curves, except for those at integral or half-integral height, which instead meet M_k in $k+1$ lines. These lines intersect in a single point and make equal angles there. This implies that M_k is invariant under rotations of order $k+1$ around the x_3-axis.

(c) In each plane at quarter- and three-quarter-integral height, there are $k+1$ equally spaced normal symmetry lines.

(d) M_k possesses $k+1$ vertical planes of reflective symmetry.

(e) Horizontal planes at quarter or three-quarter integral height are planes of reflective symmetry of M_k.

(f) The quotient surface M_k/t has genus $2k+1$ and two planar ends.

These examples have been generalized [Hoffman and Wohlgemuth] by the insertion of "Neovius handles" at the half-integral levels (Figure 5). The resulting surfaces share properties (a)–(e) above with the M_k. Their quotient by t is a surface of genus $4k+1$ with two planar ends.

No other examples—in particular, no even-genus examples at all—of singly periodic, embedded minimal surfaces with more than one end were known until the recent discovery [Wei 1991, 1992; Wei] of a family with genus-two quotients that generalizes the surfaces $\mathcal{R}$ of Riemann. Morphologically, these surfaces look like Riemann's, but they have alternating interplanar distances, and, in the narrower of the two slabs, the tube grows a handle as in the Hoffman–Wohlgemuth examples of Figure 5.

2. THE METHODS OF CONSTRUCTION

The surfaces M_k can be constructed in three ways: by a minimax procedure using a sequence of least-area annuli; by solving the Plateau problem for an appropriate polygonal boundary; and by the Weierstrass representation theorem. In [Callahan et al. 1989], all these methods are discussed.

In [Callahan et al. 1990] the existence of the $M_{k,\theta}$ is established:

Theorem 2.0 [Callahan et al. 1990]. *For every positive integer k and angle θ with $0 < |\theta| < \pi/(k+1)$, there exists a properly embedded minimal surface $M_{k,\theta}$ invariant under the screw motion s given by*

$$s\begin{pmatrix} x_1 \\ x_2 \\ x_3 \end{pmatrix} = \begin{pmatrix} \cos 2\theta & -\sin 2\theta & 0 \\ \sin 2\theta & \cos 2\theta & 0 \\ 0 & 0 & 1 \end{pmatrix}\begin{pmatrix} x_1 \\ x_2 \\ x_3 \end{pmatrix} + \begin{pmatrix} 0 \\ 0 \\ 1 \end{pmatrix}$$

and satisfying properties (a)–(c) *in Section* 1.3.

2.1. The Minimax Procedure

Theorem 2.0 was proved by a minimax procedure, generalizing the one used for the surfaces M_k. The idea is to produce a properly immersed minimal annulus bounded by $k+1$ straight lines in the planes $x_3 = 0$ and $x_3 = \frac{1}{2}$.

Lemma 2.1. *Let L_k, for $k \geq 1$, be a set of $k+1$ lines contained in the (x_1, x_2)-plane and meeting in equal angles at the origin. Let $L_{k,\theta}$ denote the image of L_k under the composition of a rotation around the x_3-axis by θ and a vertical translation by $(0, 0, \frac{1}{2})$. Then $L_k \cup L_{k,\theta}$ is the boundary of a properly immersed minimal annulus $A_{k,\theta}$ such that*

(a) *$A_{k,\theta} - \{(0,0,0), (0,0,\frac{1}{2})\}$ is an embedded surface in the slab $0 \leq x_3 \leq \frac{1}{2}$,*

(b) *$A_{k,\theta}$ is invariant under rotation around the x_3-axis by $2\pi/(k+1)$, and*

(c) *$A_{k,\theta}$ is invariant by 180° rotation around the lines obtained from L_k by first rotating around the x_3-axis by $\pi/(k+1) + \frac{1}{2}\theta$ and then translating vertically by $(0, 0, \frac{1}{4})$.*

The desired surface $M_{k,\theta}$ is produced from $A_{k,\theta}$ by Schwarz reflection around its line boundaries.

The proof of the lemma involves first finding least-area annuli bounded by "bowties" of the sort shown in Figure 6 separated by a distance $t > 0$. This solution is then rescaled so that its maximum Gauss curvature is 1 in absolute value. In this family it is shown that one can choose a sequence of solutions with $t_i \to 0$, as well as rescaling and translation factors, so that there is a subsequence that converges to the desired surface $A_{k,\theta}$.

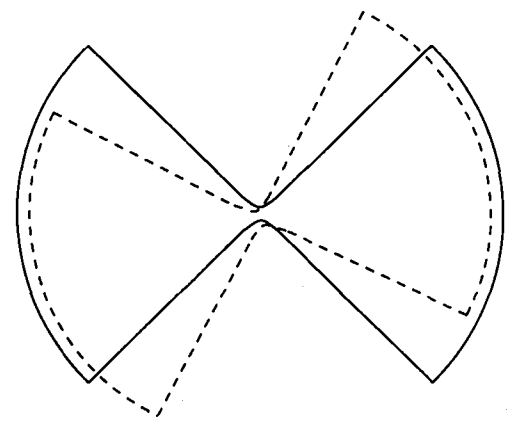

FIGURE 6. Boundary of approximant of $A_{k,\theta}$ (see Lemma 2.1, and compare Figure 11).

This method proves existence, but provides no help in establishing uniqueness. Also, the smooth dependence of $A_{k,\theta}$ (and hence $M_{k,\theta}$) on θ has not been proved, although it would follow from uniqueness of the $A_{k,\theta}$. One of our motivations in carrying out the numerical experiments described below is

to demonstrate experimentally the smooth dependence of $M_{k,\theta}$ on θ.

Moreover, the method gives no means of producing an image of $A_{k,\theta}$. While it is possible to solve numerically the boundary value problem for the bowties in Figure 6, and then let the size of the bowtie expand, this is not the procedure of the proof, and the limit surface is *not* $A_{k,\theta}$. Thus, these solutions are not close to the desired surface. In fact, it is not hard to show that the limit surface extends by Schwarz reflection to the surface in Figure 2, which does not even have planar horizontal ends. A key difference is that the basic building block obtained by numerically solving the boundary value problem is stable, whereas $A_{k,\theta}$ is not.

Remark. The existence proof given in [Callahan et al. 1990] fails when the twist angle for $A_{k,\theta}$ is equal to $\pi/(k+1)$ in absolute value. For this and other reasons, we believed that the surface $M_{k,\pi/(k+1)}$ did not exist and that, as $|\theta|$ approaches $\pi/(k+1)$, the surfaces $M_{k,\theta}$ drift off to some degenerate limit. The computations described in Section 5 were inconclusive, but did suggest that, if the surface existed in the family we constructed, it would regain reflective symmetry. In Section 6, we prove that a limit with reflective symmetry cannot exist.

2.2. The Conjugate Surface Method

Because the translation-invariant surfaces M_k possess many reflective symmetry planes, it is possible to decompose them into simply connected pieces, bounded by planar geodesic principal curvature lines. This means that the conjugate surface to the basic piece is bounded by line segments and rays (Figure 7). By solving the Plateau problem with this conjugate boundary, it is possible to prove the existence of the surfaces M_k, and such a method could be used to produce images of M_k [Callahan et al. 1989; Hoffman and Meeks 1990]. For the twisted surfaces $M_{k,\theta}$, with $0 < |\theta| < \pi/(k+1)$, there are no planes of reflective symmetry and this process cannot even be started. Moreover, the symmetries of $M_{k,\theta}$ cannot be used to find a subdomain that is stable and that will produce the surface by Euclidean motions.

2.3. The Weierstrass Representation

In subsequent sections we will develop the theory for a generalized Weierstrass representation for singly periodic minimal surfaces with planar ends and invariant under a screw motion (Section 3), describe how to apply this theory to the surfaces $M_{k,\theta}$ (Section 4), and describe the techniques and results of our numerical experiments (Section 5). As necessary background for this, we will briefly review the standard theory as applied to the untwisted examples M_k.

Recall that the Weierstrass data for a minimal immersion are a parametrizing Riemann surface and, on this surface, a meromorphic function g (conceived of as the stereographic projection of the Gauss map) and a holomorphic one-form dh (whose real part is the differential of the height function). We turn to the conditions that these data must satisfy in order to give a surface M_k.

We can work with the quotient $M_k/t \subset \mathbf{R}^3/t$, since both the Gauss map and the differential of the height function are translation-invariant, and so pass to the quotient. By Theorem 1.1(c), M_k/t can be compactified by adding a finite number of punctures, one for each end. Thus we suppose we have a compact Riemann surface $\bar{\Sigma}$, an even number of points $\mathcal{E} = \{e_1, \ldots, e_r\} \subset \bar{\Sigma}$, a meromorphic function g and a holomorphic one-form dh on $\bar{\Sigma}$, satisfying the following properties:

(i) g has a zero of order $m_i \geq 2$ at e_i, for $i < r$ odd, and a pole of order $m_i \geq 2$ at e_i, for $i \leq r$ even;

(ii) dh has a zero of order $m_i - 2$ at e_i if $m_i > 2$; it has a zero of order $|n|$ wherever g has a pole or zero of order n on $\Sigma = \bar{\Sigma} - \mathcal{E}$; and is regular everywhere else.

We set $\Phi = (\frac{1}{2}(g^{-1} - g)\,dh, \frac{1}{2}i(g^{-1} + g)\,dh, dh)$. Then

$$X(p) = \operatorname{Re} \int_{p_0}^{p} \Phi$$

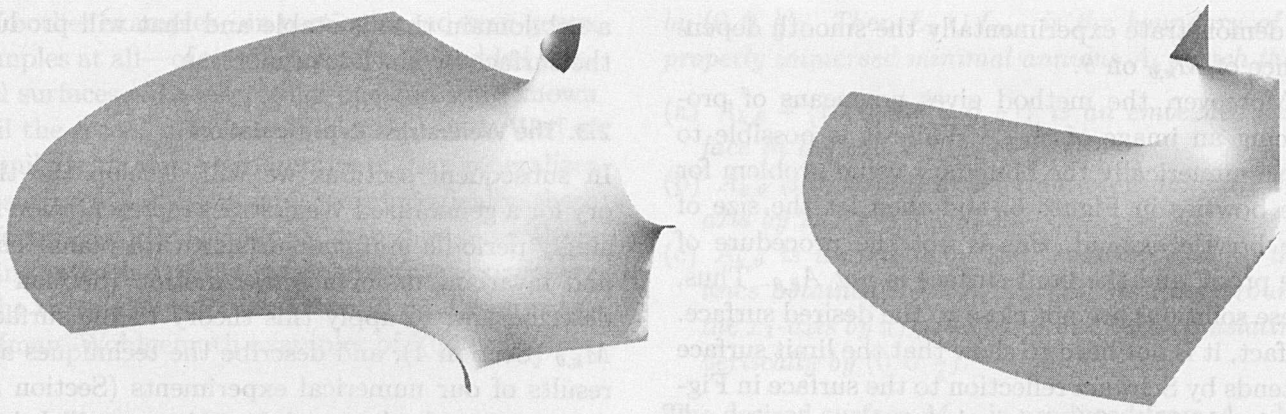

FIGURE 7. A basic piece of the surface M_1 of Figure 4, bounded by curves lying in planes of reflective symmetry, and its conjugate surface, bounded by line segments and rays.

defines a conformal, minimal, multivalued immersion of Σ into $\mathbf{R}^3$—that is, a conformal, minimal immersion of the universal cover $\tilde{\Sigma}$ of Σ into $\mathbf{R}^3$.

To recover M_k, we would like this map X to descend to a particular covering

$$\Sigma' \to \Sigma = \Sigma'/\mathbf{T},$$

where $\mathbf{T}$ is some infinite cyclic group of conformal diffeomorphisms acting freely on Σ' (this corresponds, of course, to the action of the translation t on M_k). Such a covering can be specified by giving an element Δ in $H^1(\Sigma, \mathbf{Z})$, that is, a homomorphism $H_1(\Sigma, \mathbf{Z}) \to \mathbf{Z}$. Here, if α is a closed curve in Σ, the endpoints of a lift of α to Σ' are related by $T^{\Delta([\alpha])}$, where T is a generator of $\mathbf{T}$. In fact, since the action of the translations on M_k extends to the compactification of M_k obtained by filling in points at the ends, we require that $\Sigma' \to \Sigma$ extend to a covering $\overline{\Sigma'} \to \bar{\Sigma}$, where $\mathbf{T}$ again acts freely on $\overline{\Sigma'}$. Hence the covering is specified by an element Δ in $H^1(\bar{\Sigma}, \mathbf{Z})$. For Σ' to be connected, Δ must be primitive.

The map X defines a homomorphism

$$\delta X : H_1(\bar{\Sigma}, \mathbf{Z}) \to \mathbf{R}^3,$$

whose image is a group of translational symmetries of the minimal surface $X(\tilde{\Sigma})$. We want X to descend to Σ', where the deck transformations of the covering $\Sigma' \to \Sigma$ are generated by a vertical translation. Hence the translational symmetries of $X(\tilde{\Sigma})$ should be just those we desire $X(\Sigma')$ to have, and no others. That is, if α is a closed curve in Σ and α' a lift to $\tilde{\Sigma}$, we require that the endpoints of $X(\alpha')$ differ by a vertical translation by the vector $(0, 0, \Delta([\alpha]))$. In symbols,

$$\delta X = (0, 0, \Delta). \tag{2.3.1}$$

In fact, this is nothing more than a restatement of the Weierstrass–Osserman representation theorem for complete minimal surfaces of finite total curvature, with one assumption and one modification. The assumption is that all the ends of the quotient surface in $\mathbf{R}^3/T$ are flat. The modification is the requirement that, instead of all periods of Φ being zero, there is one vertical period. For details and proofs, see [Hoffman and Karcher; Lawson 1971; Osserman 1986]. Because we wish to produce an embedded surface with planar ends, the orientation of the ends must alternate and g must be branched at the ends. This is condition (i) on the previous page. Condition (ii) is the same as in the case of finite total curvature.

In the next section, we will develop this representation in the more general setting of a surface invariant under a screw motion. Here we have described the special case when the screw motion is just a translation. The critical difference—and the one that creates all the difficulty—is that, for a

minimal surface invariant under a screw motion with nontrivial twist, the Gauss map g is not well-defined on the quotient. Thus, we cannot specify a meromorphic function to be integrated as in the case of M_k.

However, dg/g does descend to the quotient as a meromorphic one-form, which we will label μ. We can then try to reproduce S as a multivalued map from the quotient by using $\tilde{g} := \exp \int \mu$ in place of g. However, $\tilde{g}$ is itself multivalued and subject to period problems.

3. THE GENERALIZED WEIERSTRASS REPRESENTATION FOR SURFACES INVARIANT UNDER A SCREW MOTION

Suppose that S is a complete minimal surface in $\mathbf{R}^3$ invariant under the screw motion s defined in Theorem 2.0 (which has nontrivial twist). We will condense our notation, writing a point $p \in \mathbf{R}^3$ as $p = (z, x_3)$, with $z = x_1 + i x_2$, so that

$$s(z, x_3) = (e^{2i\theta} z,\ x_3 + 1).$$

Suppose S is embedded. Then, by Theorem 1.1, the quotient $\Sigma = S/s$ has finite topology if and only if it has finite total curvature, and then Σ is conformally a compact Riemann surface $\bar{\Sigma}$ punctured in a finite number of points $\mathcal{E} = \{e_1, \ldots, e_r\}$. If we assume further that S has more than one topological end, then all the annular ends of S, and therefore of $\Sigma \subset \mathbf{R}^3/s$, are planar. A planar end is conformally a punctured disk, asymptotic to a plane $x_3 = c$, and representable as a graph of the form

$$x_3 = c + \frac{a x_1 + b x_2}{|(x_1, x_2)|^2} + o(|(x_1, x_2)|^2).$$

The fact that the limit tangent plane is horizontal follows from Theorem 1.1(b), since s has a vertical translational component and a nonzero rotational component. (Note that if s were a translation, the planar ends would not have to be orthogonal to s, as the examples of Riemann show: see Figure 3 and [Callahan et al. 1989].)

In contrast with what happens for minimal surfaces invariant under a translation, the Gauss map of S does not in general descend to the compactified quotient $\bar{\Sigma}$. However, certain properties of the Gauss map on S persist in the quotient. For example, if the Gauss map g is vertical at a point $q \in S$, then $g(q) = 0$ or ∞, and likewise for $g(s^i p)$ for all $i \in \mathbf{Z}$. Hence we may speak of points of Σ as having a vertical normal, even though the Gauss map does not descend to Σ as a map to S^2. We will denote by $\mathcal{V} \subset \Sigma$ the collection of such *vertical points*. (Note that the points of $\mathcal{E} = \bar{\Sigma} - \Sigma$ also have vertical normal.) Similarly, we may speak about the *order of* g at a point of Σ.

The Gauss map g is meromorphic on S and must be branched at a planar end. Let m_i be the branching order at $e_i \in \mathcal{E}$. We will use the convention that the order of g is positive at a zero and negative at a pole. Because S is embedded, g must alternate between 0 and ∞ on the ends of S, ordered by height in $\mathbf{R}^3$. Therefore, the number of ends of $\bar{\Sigma}$ is even and the ends can be ordered so that $m_1, \ldots, m_r$ alternate in sign. Because

$$g(s^k p) = e^{2ik\theta} g(p)$$

on S, for all $k \in \mathbf{Z}$, the form $\mu := dg/g$ is well-defined on $\bar{\Sigma}$. At vertical points of $\bar{\Sigma}$, the meromorphic form μ has simple poles. The residue of μ is the order of the pole or zero of g. At a branch point of g on Σ, the form μ has a zero whose order is equal to the absolute value of the branching order of g at the point in question.

The height function x_3 on S is harmonic and its complex differential dh is holomorphic. (By the complex differential of a real-valued harmonic function f we mean $df + i\,df^*$, where f^* is the harmonic conjugate of f; although f^* is only defined locally, df^* is globally defined.) The complex differential dh has zeros precisely at the vertical points $p \in S$, of order equal to n, where $\pm n$ is the order of the zero or pole of g at p. At a planar end, dh has a zero of order $|m| - 2$, where m is the order of the zero or pole of g there. The one-form dh is clearly

invariant under the action of s and hence defines a holomorphic one-form on $\bar{\Sigma}$ with zeros at the vertical points $\mathcal{V} \subset \Sigma$, of order $|n_j|$, and zeros at ends $e_i \in \mathcal{E}$ of order $|m_i| - 2$.

To summarize the story so far:

Theorem 3.1. *Let S be a complete embedded minimal surface with more than one topological end, and invariant under a screw motion s having vertical translational component (of length 1) and nontrivial twist (of angle 2θ). Assume moreover that $\Sigma = S/s$ has finite topology.*

Then all the ends of S are planar (asymptotically horizontal), and $\Sigma = \bar{\Sigma} - \mathcal{E}$, where $\bar{\Sigma}$ is a compact Riemann surface and $\mathcal{E} = \{e_1, \ldots, e_r\}$ is a finite set, which we index (cyclically) in order of increasing height of the corresponding ends of S.

Let $g : S \to \mathbf{C} \cup \{\infty\}$ be the stereographic projection of the Gauss map of S, and x_3 the height function on S. Then $\mu = dg/g$ is a meromorphic one-form, and $dh = dx_3 + i\,dx_3^*$ is a holomorphic one-form on S. They descend to a meromorphic and a holomorphic one-form on $\bar{\Sigma}$, satisfying the following conditions:

(a) *All poles of μ on $\bar{\Sigma}$ are simple and have integer residues. They fall into two groups: the points e_i, for $i, \ldots, r$, with residues m_i that alternate in sign; and other points $v_1, \ldots, v_s \in \Sigma$, called vertical points, whose residues we denote by n_j, for $j = 1, \ldots, s$.*

(b) *The one-form dh is holomorphic on $\bar{\Sigma}$ and its zeros on Σ are precisely the vertical points v_j, for $j = 1, \ldots, s$, and have order $|n_j|$. The remaining zeros of dh are the points $e_i \in \mathcal{E}$ where $|m_i| > 2$, and have order $|m_i| - 2$.*

The total curvature of Σ is $-4\pi(k + r - 1)$, where k is the genus of $\bar{\Sigma}$, and we have

$$\sum_1^s |n_j| + \sum_1^r |m_i| = 2(r + k - 1). \tag{3.1}$$

This last formula is simply the Euler characteristic of $\bar{\Sigma}$, computed by summing the zeros of dh.

Because the translational part of s has length 1, the integral of dh along a closed curve α on Σ must be an integer. It is straightforward to verify that the vertical displacement map $\Delta : H_1(\Sigma, \mathbf{Z}) \to \mathbf{Z}$ given by

$$\Delta([\alpha]) = \int_\alpha dh \tag{3.2}$$

is well-defined and an additive homomorphism.

Locally, $g = \exp \int dg/g$ on S. Suppose α is a closed curve on Σ. Then

$$F(\alpha) := \exp \int_\alpha \frac{dg}{g}$$

is the ratio of the values of g at the endpoints of any lift of α to S. Endpoints are related by the action of $s^{\Delta([\alpha])}$, so $F(\alpha)$ is unitary. Clearly this gives a multiplicative homomorphism

$$F : H_1(\Sigma, \mathbf{Z}) \to S^1,$$

with

$$F([\alpha]) = \exp(2i\Delta([\alpha])\theta), \tag{3.3}$$

where 2θ is the twist angle of s.

The metric on S is given by

$$ds = \tfrac{1}{2}(|g| + |g|^{-1})\,|dh|.$$

The completeness of S is equivalent to the condition

$$\int_\alpha (|g| + |g|^{-1})\,|dh| = \infty,$$

where α is any path in Σ with $\lim_{t\to\infty} \alpha(t) \in \mathcal{E} \subset \bar{\Sigma}$.

The Gauss map g of S may be realized on $\bar{\Sigma}$ by $\tilde{g} = \exp \int \mu$, which is a multivalued meromorphic mapping from $\bar{\Sigma}$ to $\mathbf{C} \cup \{\infty\}$, and may be used to reconstruct S by the Weierstrass representation. That is, if we set

$$\Phi = (\tfrac{1}{2}(\tilde{g}^{-1} - \tilde{g})\,dh,\ \tfrac{1}{2}i(\tilde{g}^{-1} + \tilde{g})\,dh,\ dh), \tag{3.4}$$

the mapping defined by

$$X(p) = \mathrm{Re} \int_{p_0}^{p} \Phi \tag{3.5}$$

is a multivalued conformal minimal embedding and its image is S. Specifically, if α is a closed curve on Σ and α' is a lift of α to the universal cover $\tilde{\Sigma}$, with endpoints p_0 and p_1, then

$$X(p_1) = s^{\Delta([\alpha])}p_0. \tag{3.6}$$

This relation is analogous to (2.3.1) in the translational case: it implies that the minimal immersion $\tilde{\Sigma} \to \mathbf{R}^3$ descends to a minimal immersion $\Sigma' \to \mathbf{R}^3$, where Σ' is the covering specified by the cohomology class Δ.

We can now state the converse of Theorem 3.1:

Theorem 3.2. *Suppose one has a compact Riemann surface $\bar{\Sigma}$, finite sets $\mathcal{E} = \{e_1 \dots e_r\} \subset \bar{\Sigma}$ and*

$$\mathcal{V} = \{v_1 \dots v_s\} \subset \Sigma = \bar{\Sigma} - \mathcal{E},$$

integers m_i for $1 \le i \le r$ and n_j for $1 \le j \le s$, a meromorphic one-form μ on $\bar{\Sigma}$, a holomorphic one-form dh on $\bar{\Sigma}$, a cohomology class $\Delta \in H^1(\Sigma, \mathbf{Z})$, and an angle θ, all such that equations (3.1)–(3.3) *and properties* (a)–(b) *of Theorem* 3.1 *are satisfied.*

Then the multivalued function $\tilde{g} = \exp \int \mu$ yields a multivalued, conformal, minimal immersion X by (3.4)–(3.5). *That is, it yields a conformal minimal immersion $\tilde{\Sigma} \to \mathbf{R}^3$, where $\pi : \tilde{\Sigma} \to \Sigma$ is the universal cover of Σ. The image $S = X(\tilde{\Sigma})$ is invariant under s, all its annular ends are planar ends, its vertical points are $X(\pi^{-1}\mathcal{V})$, and its ends are $\pi^{-1}\mathcal{E}$.*

If (3.6) *holds, X will descend to a proper immersion of the covering Σ' of Σ specified by Δ. This immersion restricts to an embedding of a small punctured neighborhood of each point $e_i \in \mathcal{E}$, having as image a planar end of S/s.*

Note that, although X is an embedding near the punctures, it need not be globally one-to-one, so $X(\Sigma') \subset \mathbf{R}^3$ may fail to be embedded.

4. THE GENERALIZED WEIERSTRASS REPRESENTATION OF THE SURFACES $M_{k,\theta}$

We wish to find the Weierstrass representation for the surfaces $M_{k,\theta}$ having the properties stated in Theorem 2.0. For the moment, we assume that the surface, as described, exists (as indeed it does by the theorem). We will use its geometric properties to deduce its Weierstrass representation. Once this is done, we must verify that this representation, with an appropriate choice of parameters, actually produces a surface with the required properties.

4.1. Symmetry and the Underlying Riemann Surface

The screw motion $s(x_1 + ix_2, x_3) = (e^{2i\theta}(x_1 + ix_2), x_3 + 1)$ acts on the minimal surface $M_{k,\theta}$ in such a way that the quotient is a surface $\Sigma = M_{k,\theta}/s$ of genus $2k+1$, with two planar ends in the space form $\mathbf{R}^3/s$. The surface has further symmetries that descend to the quotient Σ:

(i) the rotation ρ around the x_3-axis by an angle $2\pi/(k+1)$;
(ii) the 180° rotations around the other (horizontal) normal symmetry lines, of which there are $k+1$ at each level halfway between neighboring ends (at heights $\frac{1}{4} + \frac{1}{2}\mathbf{Z}$);
(iii) the 180° rotations about the lines on the surface, of which there are $k+1$ at each half-integer height (each $(k+1)$-tuple of lines meets on the x_3-axis, and these are the only points of the surface on the x_3-axis).

The generalized Weierstrass data dg/g and dh are invariant under the rotations around the x_3-axis, and therefore pass to the quotient $\bar{\Sigma}/\rho$. Note that the Weierstrass representation produces the minimal surface by integration of differential forms; if these forms are lifts from a quotient surface, we might as well determine and integrate these forms on the quotient. This is a simplification, since the Riemann–Hurwitz formula

$$2 - 2(2k+1) = \chi(\bar{\Sigma}) = (k+1)\,\chi(\bar{\Sigma}/\rho) - 4k$$

implies that the quotient $T := \bar{\Sigma}/\rho$ is a torus, independent of k. Moreover, this torus is rectangular, as the following symmetry argument shows.

As stated under (iii) above, $M_{k,\theta}$ has $k+1$ horizontal straight lines through each point where it meets the x_3-axis. Each such $(k+1)$-tuple of lines

gives one line in T. The 180° rotations of $M_{k,\theta}$ around these lines give an orientation-reversing involution of T. The vertical points of $M_{k,\theta}$ project to two points on $\bar{\Sigma}$ that are fixed by ρ, and hence they project to two points on T. Therefore, the lines on $M_{k,\theta}$ project to two disjoint components of the fixed-point set of an orientation-reversing involution of T. Such an involution only exists on a rectangular torus, where it can be visualized as a reflection in, say, two horizontal lines in the fundamental rectangle (dashed in Figure 8).

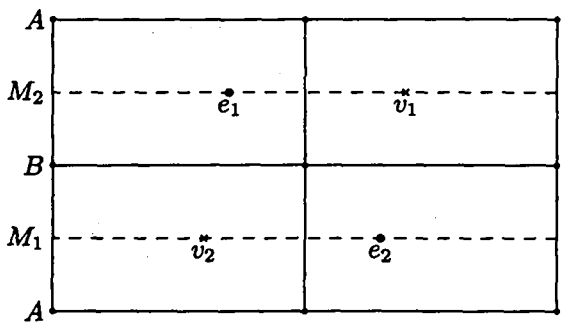

FIGURE 8. Portrait of $T = \bar{\Sigma}/\rho$, obtained by symmetry considerations. The dashed lines form the fixed-point set of an orientation-reversing involution of T, coming from the lines of $M_{k,\theta}$. The form dg/g is real on these lines. Its poles are at the vertical points v_1, v_2 and at the ends e_1, e_2.

Thus, using symmetry considerations alone, we have greatly narrowed down the possibilities for the Riemann surfaces on which the Weierstrass forms are to be constructed. We still have one free real parameter, the modulus of the torus, which will be a free parameter in the representation.

On each line in the fixed-point set just discussed there is a point coming from a vertical point on Σ and a point coming from a planar end. Together with the modulus of the rectangular torus, this would give five real parameters to be determined. However, additional symmetry considerations will further reduce this number to three.

Consider rotations around the horizontal normal symmetry lines at quarter-integral heights $\frac{1}{4} + \frac{1}{2}\mathbf{Z}$. They descend to a single orientation-preserving involution r of T that fixes four points and interchanges the two dashed lines of Figure 8. This involution must be 180° rotation about the four fixed points in the torus, which we can choose, without loss of generality, to be the half-period points. Thus the dashed lines must pass through quarter-period points. Since the involution r interchanges the two ends, the position of the end on one of the dashed lines determines its position on the other. In other words, the ends are symmetrically placed, as indicated in Figure 8. The same is true of the vertical points. Hence, three independent real parameters are sufficient to fix the conformal structure and the position of the ends and vertical points.

We observe that, by the Riemann–Hurwitz formula, the torus modulo the involution r is a sphere. This fact will be important later on.

4.2. The Differential Forms dh and dg/g

The Gauss map of $M_{k,\theta}$ has order k at the vertical points and order $k+2$ at the planar ends. This means that dh on $\bar{\Sigma}$ has zeros of order k at these points. Since the branching order of $\bar{\Sigma} \to T$ is $k+1$ at these points, this shows that dh descends to a *holomorphic* form on T. Hence there are no further choices: dh is a constant multiple of the translation-invariant, standard differential form on the torus: $dh = c\,du$, where $u \in T = \mathbf{C}/\Gamma$ and c is a nonzero complex constant. The magnitude of c is irrelevant: it merely rescales the surface. However, the real part of dh must be zero when applied to tangent vectors of the horizontal lines in T that correspond to the lines in the surface, since $x_3 = \operatorname{Re} \int dh$. Hence c must be purely imaginary. Without loss of generality, we assume that $c = i$, that is,

$$dh = i\,du. \tag{4.2.1}$$

We know from Theorem 3.1 that the one-form dg/g on $\bar{\Sigma}$ has simple poles at the vertical points and ends. The residue of dg/g is the order of the pole or zero of g. In our case, the residue at a vertical point in Σ is $\pm k$ and the residue at an end is $\pm(k+2)$. As observed in Section 4.1, dg/g passes to

the quotient T, and there it has simple poles at the points v_1, v_2, e_1, e_2 (Figure 8). Since the branching order of $\bar{\Sigma} \to T$ is $k+1$ at these points, the residues become $\pm k/(k+1)$ at v_1, v_2 and $\pm(k+2)/(k+1)$ at e_1, e_2. Using this information, we will now write down a formula for dg/g in terms of elliptic functions on T.

4.3. The elliptic function Z

We remarked at the end of Section 4.1 that T/r is conformally S^2. After we fix an identification of S^2 with $\mathbf{C} \cup \{\infty\}$, we may consider the projection $T \to T/r = S^2$ to be an elliptic function Z of degree two. We will choose this identification as follows. The projection of the vertex A of the rectangle goes to ∞, and the projection of the midpoint B of the vertical edge goes to zero. The midpoints M_1, M_2 between these points project to a single point on S^2, which we choose to be -1. Now

$$Z : T \to S^2 = \mathbf{C} \cup \{\infty\}$$

is a well-defined elliptic function.

Consider the symmetries of Z. Denote by R the reflection in either the horizontal or the vertical line through B. Then R fixes B and A, and it either interchanges or fixes M_1 and M_2. In either case Z and $Z \circ R$ coincide on

$$\{A, B, M_1, M_2\} = Z^{-1}(\{0, \infty, -1\});$$

since the involution R is antiholomorphic, this implies that $Z \circ R = \iota \circ Z$, where ι denotes complex conjugation, and that Z is real on the fixed-point set of R. Recalling the definition of R, we see that Z is real along all the solid lines of Figure 8, and in particular at the other two branch points of Z, which are the center of the rectangle and the midpoint of its horizontal edge.

Similarly, consider the reflection R' in the horizontal line through M_1, which is also the reflection in the horizontal line through M_2, and corresponds in $M_{k,\theta}$ to 180° rotations about the horizontal lines contained in this surface. R' interchanges B and A and fixes M_1 and M_2. Hence $Z \circ R' = \iota' \circ Z$, where ι' is the map $z \mapsto \bar{z}^{-1}$ of S^2. Thus Z maps the fixed-point set of R' (the dashed lines of Figure 8) to the unit circle. In particular, the other branch values of Z are also symmetric with respect to the unit circle, and we name them $\lambda \leq \lambda^{-1} \in \mathbf{R}^+$.

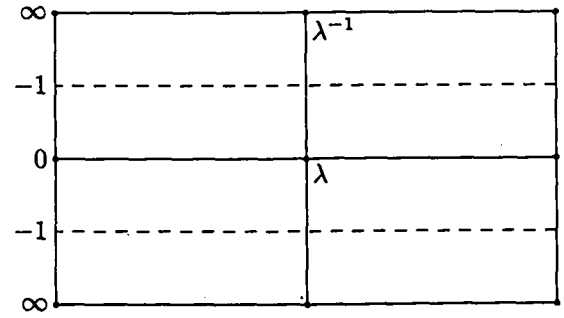

FIGURE 9. Values of the elliptic function Z on the fundamental rectangle. The branch values are $0, \infty, \lambda \leq \lambda^{-1}$. Solid lines indicate the locus of Z real, and dashed lines the locus of Z unitary.

We summarize what we know so far about Z (see also Figure 9):

(i) The composition

$$M_{k,\theta} \to M_{k,\theta}/s = \bar{\Sigma} \to \bar{\Sigma}/\rho = T \xrightarrow{Z} S^2 = \mathbf{C} \cup \{\infty\}$$

is a meromorphic function on $M_{k,\theta}$.

(ii) Z is unitary on horizontal lines of $M_{k,\theta}$.

(iii) The $4(k+1)$ points fixed under the 180° rotations of $\bar{\Sigma}$ about the horizontal normal symmetry lines are mapped to the four (real) branch values of Z, which are $0, \infty, \lambda, \lambda^{-1}$, for some $\lambda \in (0, 1)$.

The function Z is well-adapted (although not perfectly, as we shall see) to the symmetry of $M_{k,\theta}$. We remark that the Weierstrass $\wp$-function on T has the same branch points as Z. It is normalized by its Mittag-Leffler expansion, while we wish Z to be adapted to our minimal surface. Because they both have the same double pole, we have $Z = c\wp + d$, for some complex constants c, d.

The logarithmic derivative Z'/Z is again an elliptic function; it has two simple poles at the double zero and double pole of Z, and two simple zeros

at the other branch points of Z. The functions $(Z'/Z)^2$ and $Z + Z^{-1} - \lambda - \lambda^{-1}$ are therefore proportional. The proportionality factor is real, and positive since both functions are positive on the horizontal line through B. This factor is irrelevant to our discussion, and by scaling the fundamental rectangle we can make it equal to 1. Then we have

$$\left(\frac{Z'}{Z}\right)^2 = Z + \frac{1}{Z} - \lambda - \frac{1}{\lambda},$$

$$Z'^2 = Z^3 - \left(\lambda + \frac{1}{\lambda}\right) Z^2 + Z,$$

for some $\lambda \in \mathbf{R}$. This is the classical description of a (rectangular) torus as a cubic curve (with conformal parameter λ). We consider a choice of λ as specifying a particular torus and the differential equation as defining a doubly periodic function (in fact a family $Z_a(u) := Z(u + a)$).

4.4. The One-Form dg/g in Terms of Z

Recall that on $M_{k,\theta}$ the Gauss map has zeros and poles of order k at the finite vertical points and zeros and poles of order $k + 2$ at the punctures. Therefore, the differential of dg/g on both $M_{k,\theta}$ and $M_{k,\theta}/s = \bar{\Sigma}$ has simple poles with residues $\pm k$ and $\mp(k + 2)$. On $\bar{\Sigma}$, each puncture is joined to one of the (two) vertical points by $k + 1$ horizontal lines and the residues there have opposite sign, since the Gauss map points in opposite directions. We noted that the projection of the vertical points of Σ and the projection of the planar ends in $\bar{\Sigma}$ both lie on the projection of the lines that lie in $\bar{\Sigma}$, on which Z is unitary. We labeled the image in T of the vertical points by v_1, v_2, and the image of the ends by e_1, e_2 (Figure 8). We also noted in Section 4.2 that these points are symmetric with respect to the order-two rotation r about the half-periods. We may specify these geometrically determined points by means of two unitary numbers e and v:

$$Z(e_1) = Z(e_2) = e,$$
$$Z(v_1) = Z(v_2) = v.$$

From the differential equation for Z and the relation $Z \circ r = Z$, we have

$$Z'(e_1) = -Z'(e_2) = \pm\sqrt{e^2(e + e^{-1} - (\lambda + \lambda^{-1}))},$$
$$Z'(v_1) = -Z'(v_2) = \pm\sqrt{v^2(v + v^{-1} - (\lambda + \lambda^{-1}))}.$$

Knowing the zeros, poles and residues of dg/g, we can determine dg/g in terms of Z. Let u be the standard coordinate on $\mathbf{C}/\Gamma = T$. Then $dZ = Z'\,du$, and $du = dZ/Z'$ has neither zeros nor poles on T. We must have

$$\frac{dg}{g} = \left(-\frac{k+2}{k+1}\frac{Z'(e_1)}{Z-e} + \frac{k}{k+1}\frac{Z'(v_1)}{Z-v} + c\right)\frac{dZ}{Z'}. \quad (4.4.1)$$

We now have the generalized Weierstrass representation for our minimal surfaces:

$$g = \exp\int \frac{dg}{g}, \quad (4.4.2)$$

$$X(p) = \int_{p_0}^{p} (\tfrac{1}{2}(g^{-1} - g),\ \tfrac{1}{2}i(g^{-1} + g),\ 1)\,dh, \quad (4.4.3)$$

where $dh = i\,du$ (see (4.2.1)). These data contain a real parameter $\lambda \in \mathbf{R}$, two unitary parameters $e, v \in e^{i\mathbf{R}}$, and one complex parameter c.

4.5. Geometric Properties of the Derived Minimal Surfaces

The horizontal straight lines on T are mapped to level lines of the image $X(T)$, since the third component of the Weierstrass representation is constant along these lines. Along the horizontal lines in T that correspond to the straight lines on the minimal surface in $\mathbf{R}^3$, the differential dg/g must have real values, because g on these lines takes values on a line through 0 in $\mathbf{C} \cup \{\infty\}$. But it is not clear that our expression has this property. On the other hand, numerical experimentation indicates that the values do come out real! It turns out that the $\wp$-function, which was our guide for the normalization of Z, was not a perfect choice. Instead we should have mapped the preimages in

T of those horizontal lines to $\mathbf{R}$ rather than $e^{i\mathbf{R}}$. We correct this with the Möbius transformation

$$m(z) := \frac{z - e^{i\alpha}}{1 - e^{i\alpha}z},$$

which interchanges $\mathbf{R}$ and $e^{i\mathbf{R}}$:

$$m(0) = -e^{i\alpha}, \quad m(\infty) = -e^{-i\alpha}, \quad m(-1) = -1.$$

The most symmetric situation is achieved if we send the other two branch values, λ and λ^{-1}, to $e^{-i\alpha}$ and $e^{i\alpha}$, respectively. This requires α to satisfy

$$e^{-i\alpha}(1 - e^{i\alpha}\lambda) = \lambda - e^{i\alpha},$$

which is the case if we choose α such that $\cos\alpha = \lambda$. Thus we will replace the elliptic function Z by the Jacobi-type elliptic function $\mathfrak{J} := m \circ Z$ (see Figure 10).

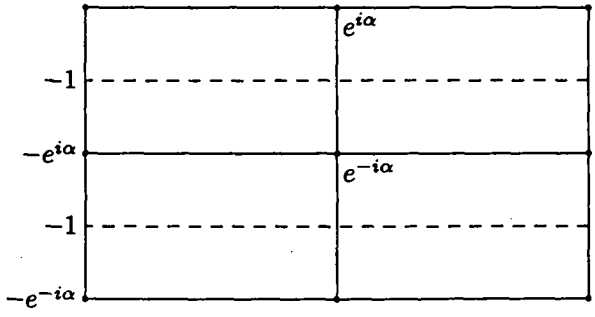

FIGURE 10. Values of the elliptic function $\mathfrak{J}$ on the fundamental rectangle. The branch values are $\pm e^{\pm i\alpha}$. Dashed lines indicate the locus of $\mathfrak{J}$ real, and vertical solid lines the locus of $\mathfrak{J}$ unitary.

The function $\mathfrak{J}$ has branch values $\pm e^{\pm i\alpha}$, where $\cos\alpha = \lambda$. We define $E := m(e) \in \mathbf{R}$ and $V := m(v) \in \mathbf{R}$ to be the special values of $\mathfrak{J}$; then the equation (4.4.1) for dg/g is replaced by

$$\frac{dg}{g} = \left(-\frac{k+2}{k+1}\frac{\mathfrak{J}'(e_1)}{\mathfrak{J}-E} + \frac{k}{k+1}\frac{\mathfrak{J}'(v_1)}{\mathfrak{J}-V} + c\right)\frac{d\mathfrak{J}}{\mathfrak{J}'}. \quad (4.5.1)$$

Along the lines on T in question, $d\mathfrak{J}/\mathfrak{J}' = du$ is real (on the tangent vectors), $\mathfrak{J}$ is real and the constants E, V, $\mathfrak{J}'(e_1)$, $\mathfrak{J}'(v_1)$ are also real. Therefore, we have to choose c real. With these choices, $\tilde{g} = \exp(\int dg/g)$ has values on a fixed meridian of T, that is, reflection in the special lines on T is an isometry of the Riemannian metric

$$ds = \frac{1}{2}\left(|g| + \frac{1}{|g|}\right)|dh|.$$

Therefore, these lines are geodesics on the surface. The second fundamental form is given by the real part of the quadratic form $(dg/g)\cdot dh$, which takes on values in $i\mathbf{R}$ on the tangent vectors to these geodesics. Therefore, these geodesics have no normal curvature (they are asymptotic lines), and must be straight lines in $\mathbf{R}^3$, as desired.

Next, we choose c so that the horizontal period of dg/g is also imaginary. We may do this explicitly in terms of elliptic integrals. We have no more parameters to adjust this imaginary period to $2\pi i/(k+1)$, but the residues help us: if we move the horizontal generator towards the symmetry line containing e_1 and v_1 (see Figure 8), then, since $\mathfrak{J}$ is real on this line (as is du), we pick up half the residues of the poles of dg/g at e_1 and v_1. The situation for the other symmetry line is similar. Thus the period is

$$\frac{\pm 2\pi i}{2}\left(\frac{k+2}{k+1} - \frac{k}{k+1}\right) = \pm\frac{2\pi i}{k+1},$$

as needed.

The screw motion s and the rotation ρ of $M_{k,\theta}$ do not change the absolute value of g, but only its phase: g becomes $e^{i\theta}g$ under s and $e^{2\pi i/(k+1)}g$ under ρ. Therefore, the period of dg/g should be $i\theta$ on a vertical generator of T and $2\pi i/(k+1)$ on a horizontal generator. Now $du = d\mathfrak{J}/\mathfrak{J}'$ is imaginary on the vertical generator and $\mathfrak{J}$ has complex conjugate values at points symmetric with respect to the symmetry lines $\mathfrak{J}^{-1}(\mathbf{R})$. The vertical period of dg/g is therefore imaginary. (Note that c has already been chosen to be real.) The value $i\theta$ of this period depends on $\lambda = \cos\alpha$. In the next section we will determine E and V as functions of λ. We do not need to specify this dependence. We now know that the Weierstrass data (4.2.1) and (4.4.1) will produce a surface with the desired symmetries, provided we can solve the period problem.

4.6. The Period Problem

In Sections 4.1–4.5 we derived a three-parameter family of minimal surfaces that have all the desired symmetry properties of the family $M_{k,\theta}$. What remains to be shown is the existence of parameters for which the Weierstrass representation (3.4)–(3.5), which is multivalued on T, defines a mapping on $\bar{\Sigma}$ that has a single period, corresponding to the desired screw motion s. (See Theorems 3.1 and 3.2.)

Half the horizontal generator of T that joins the branch points where $Z = 0$ and $Z = \lambda$ is mapped to a level line on the minimal surface. At the endpoints of this level line, the surface normals are symmetry normals meeting at an angle $\pi/(k+1)$ at a point that we will call $Q \in \mathbf{R}^3$. The 180° rotation around these normals continues the surface analytically, and extends the level line to a closed waist curve on the minimal surface. There is no period problem here.

Next we consider the image of a wider and wider band around this level line. Near the point v_1, the boundary level lines of the band converge to two half-lines that meet at a vertical point with an angle $\pi/(k+1)$. This point must be vertically above the point Q where the symmetry normals of the waist line meet; if this is the case, it is also true for pieces of the surface obtained by symmetry operations from the first one. Therefore we have a two-dimensional period problem: the parameters e and v have to be chosen in such a way that the horizontal lines meet vertically above Q.

The existence proof for solving this period problem is conceptually easy. The previous formulas allow us to find an approximate solution (e_1, v_1) on the computer. Then one has to take a (possibly large) circle around (e_1, v_1) in the parameter domain and prove that the corresponding intersection points of the horizontal lines form a curve with nonzero winding number with respect to $0 \in \mathbf{R}^2$. Then 0 is in the image of our parameter map and the period problem is solved.

In some situations, such an argument can be pushed through. In the present case, we have not done it "by hand"; but we can see that the accurately computed image curve does enclose the origin.

5. THE NUMERICAL COMPUTATIONS

The numerical attack on the problem consists of two steps. First, we use a program to calculate parameter values (λ, e, v) for which the period, as described above, vanishes. Then we use these parameter values to obtain pictures of the surface itself.

Both steps require performing the integration in the Weierstrass representation (4.4.1)–(4.4.3). We do this using a straightforward Gaussian quadrature routine. As is the case for other, simpler examples, the integrands involve functions defined on a branched cover of S^2, rather than on S^2 itself. Care must be taken to stay on the same branch of Z' (which is defined in Section 4.3). This example differs from earlier ones in that g is itself defined by an integral, rather than as an algebraic combination of Z and Z'. The routine that computes g integrates dg/g from the last calculated point; therefore, one must be careful to start all the integration paths from points where the value of g is already known.

To calculate the period for particular values of (λ, e, v), we integrate first from $Z = 0$ to $Z = \lambda$. We may assume that g, which is unitary at $Z = 0$, has the value 1 there. This integral fixes the point Q, defined in Section 4.6, to lie at the origin. We can then integrate from $Z = 0$ to two points on either side of v on the unit circle $|Z| = 1$. These points and the values of the Gauss map there fix the location in $\mathbf{R}^3$ of the lines on the surface. As described in Section 4.6, the period problem is solved when the intersection of these lines lies above Q.

To solve the period problem, we used a program that minimized $x^2 + y^2 + (\theta - \theta_0)^2$, where (x, y) is the period vector, θ is the calculated twist angle, and θ_0 is a desired twist angle, set beforehand. The minimization algorithm we used was the downhill

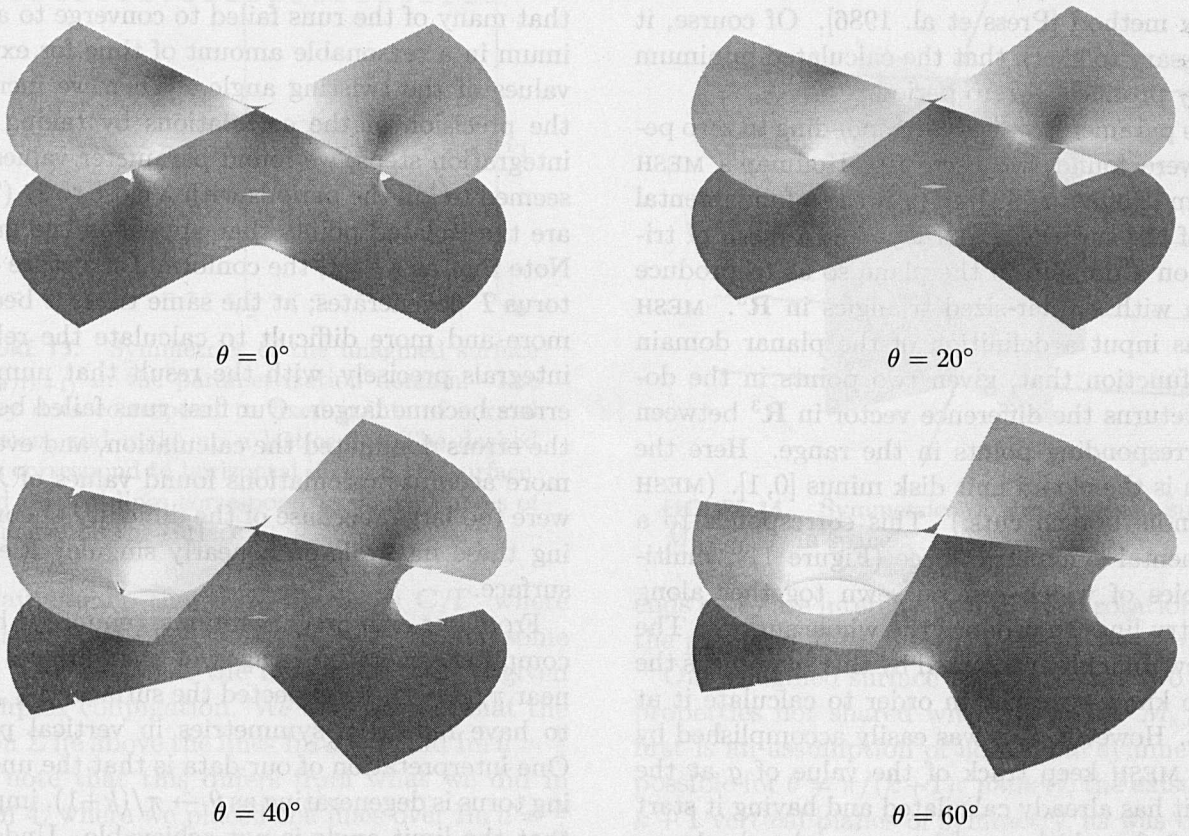

FIGURE 11. Basic pieces of $M_{1,\theta}$, for increasing values of θ (compare Figure 1). Each piece corresponds to half of the parametrization domain, such as the region between the dashed lines in Figure 8.

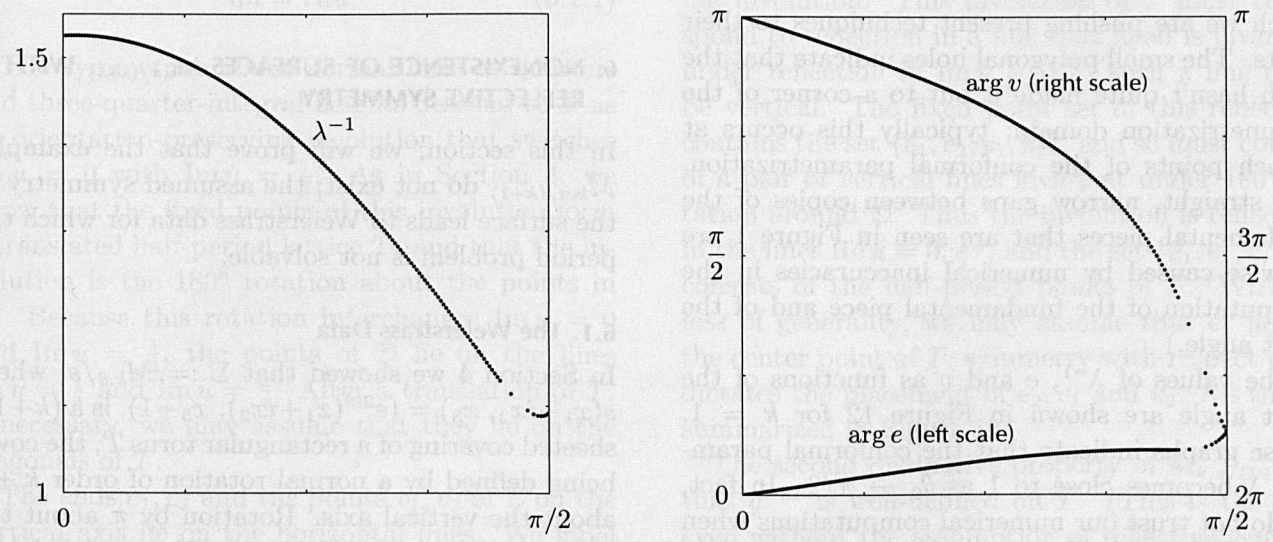

FIGURE 12. Numerical results for $k = 1$. Left: calculated values of λ^{-1} versus θ. Right: the unitary numbers e and v versus θ. As θ approaches $\pi/2$, the values of e and v tend toward complex conjugate numbers.

simplex method [Press et al. 1986]. Of course, it is necessary to check that the calculated minimum actually produces a zero period.

Once parameter values corresponding to zero periods were found, we used Jim Hoffman's MESH program [Hoffman 1993] to produce a fundamental piece of the surface. MESH lays out a mesh of triangles on a domain in the plane so as to produce a mesh with similar-sized triangles in $\mathbf{R}^3$. MESH takes as input a definition of the planar domain and a function that, given two points in the domain, returns the difference vector in $\mathbf{R}^3$ between the corresponding points in the range. Here the domain is the closed unit disk minus $[0, 1]$. (MESH can handle branch cuts.) This corresponds to a fundamental symmetric piece (Figure 11), multiple copies of which can be sewn together along symmetry lines to produce the whole surface. The only new difficulty presented by this example is the need to know g nearby in order to calculate it at a point. However, this was easily accomplished by having MESH keep track of the value of g at the points it has already calculated and having it start at $Z = 0$, for which g can be assumed to be 1.

(When the fundamental symmetric pieces are put together as in Figure 1, slight defects become apparent. These glitches illustrate the degree to which we are pushing present techniques to their limits. The small polygonal holes indicate that the mesh hasn't quite made it out to a corner of the parametrization domain; typically this occurs at branch points of the conformal parametrization. The straight, narrow gaps between copies of the fundamental pieces that are seen in Figure 1 are likewise caused by numerical inaccuracies in the computation of the fundamental piece and of the twist angle.)

The values of λ^{-1}, e and v as functions of the twist angle are shown in Figure 12 for $k = 1$. These graphs indicate that the conformal parameter λ becomes close to 1 as $\theta_0 \to \pi/2$. In fact, we do not trust our numerical computations when the twist angle is near the limit; the theoretically correct value of λ should approach 1. We observed that many of the runs failed to converge to a minimum in a reasonable amount of time for extreme values of the twisting angle. When we increased the precision of the calculations by taking more integration steps, we found parameter values that seemed to kill the periods with λ close to 1. (These are the isolated points that appear in the graph.) Note that as $\lambda \to 1$, the conformal structure of the torus T degenerates; at the same time, it becomes more and more difficult to calculate the relevant integrals precisely, with the result that numerical errors become larger. Our first runs failed because the errors dominated the calculation, and even the more accurate calculations found values of λ that were too large, because of the difficulty of computing these integrals on a nearly singular Riemann surface.

From our own preconceptions, reinforced by the computer-generated images of the surfaces for θ near $\pi/(k+1)$, we expected the surfaces $M_{k,\pi/(k+1)}$ to have reflection symmetries in vertical planes. One interpretation of our data is that the underlying torus is degenerating as $\theta \to \pi/(k+1)$, implying that the limit angle is not achievable. Under the assumption of the existence of reflection symmetry in vertical planes, we prove that, in fact, the limit is not achievable.

6. NONEXISTENCE OF SURFACES $M_{k,\pi/(k+1)}$ WITH REFLECTIVE SYMMETRY

In this section, we will prove that the examples $M_{k,\pi/(k+1)}$ do not exist; the assumed symmetry of the surface leads to Weierstrass data for which the period problem is not solvable.

6.1. The Weierstrass Data

In Section 4 we showed that $\Sigma := M_{k,\theta}/s$, where $s(x_1+ix_2, x_3) = (e^{2i\theta}(x_1+ix_2), x_3+1)$, is a $(k+1)$-sheeted covering of a rectangular torus T, the cover being defined by a normal rotation of order $k+1$ about the vertical axis. Rotation by π about the horizontal lines in $M_{k,\theta}$, at half-integral heights, induces an orientation-reversing involution of T.

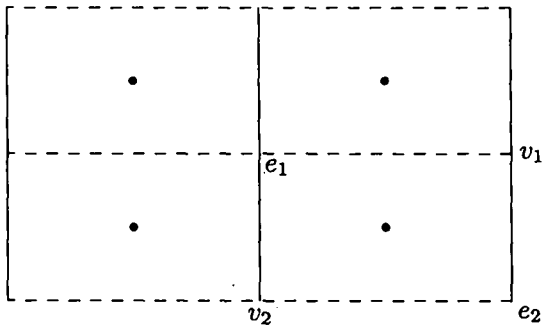

FIGURE 13. Symmetries of the imagined surface $M_{k,\pi/(k+1)}$ in the parametrization domain. The heavy dots correspond to fixed points of normal rotation, and make up a lattice $\mathcal{D}$. The dashed lines correspond to horizontal lines on the surface. Solid vertical lines correspond to planar curves of symmetry on the surface.

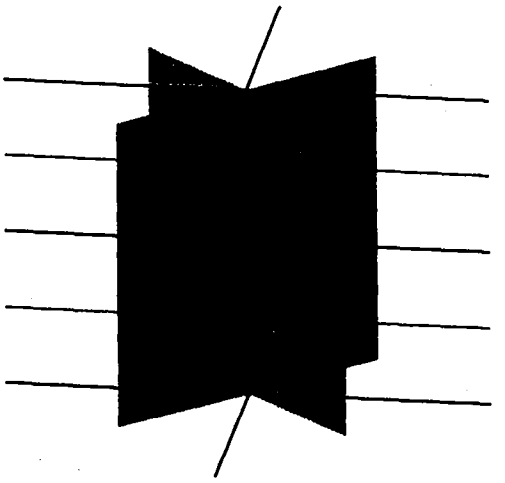

FIGURE 14. Symmetries of the imagined surface $M_{1,\pi/(k+1)}$ in space.

We may assume that T is the torus $\mathbf{C}/\Gamma$, where Γ is the lattice $\{m\tau + ni \mid m, n \in \mathbf{Z}\}$ for some real $\tau > 0$, and that the involution of T is given by complex conjugation. We also assume that the lines on Σ lie above the lines $\operatorname{Im} u = 0$ and $\operatorname{Im} u = \frac{1}{2}$ in T; note that this differs from what we did in Section 4, where we placed the lines over $\operatorname{Im} u = \frac{1}{4}$ and $\operatorname{Im} u = \frac{3}{4}$ (see Figure 13). As in Section 4, dh descends to T and must be given by

$$dh = i\,du. \tag{6.1.1}$$

The symmetries about normal lines at quarter- and three-quarter-integral heights descend to T as an orientation-preserving involution that switches $\operatorname{Im} u = 0$ with $\operatorname{Im} u = \frac{1}{2}$. As in Section 4, we know that the fixed points of this involution form a translated half-period lattice $\mathcal{D}$, and that the involution is the 180° rotation about the points in $\mathcal{D}$. Because this rotation interchanges $\operatorname{Im} u = 0$ and $\operatorname{Im} u = \frac{1}{2}$, the points of $\mathcal{D}$ lie on the lines $\operatorname{Im} u = \frac{1}{4}$ and $\operatorname{Im} u = \frac{3}{4}$. After a translation of T, if necessary, we may assume that they lie on the diagonals of T.

The ends e_1, e_2 and the points v_1, v_2 of Σ on the vertical axis lie on the horizontal lines. We label them so that $\{e_1, v_1\}$ lies on the lines over $\operatorname{Im} u = \frac{1}{2}$ and $\{e_2, v_2\}$ lies on the lines over $\operatorname{Im} u = 0$. The ends e_1, e_2 are interchanged by 180° rotation about the points in $\mathcal{D}$, as are the vertical points v_1, v_2.

Our imagined surface $M_{k,\pi/(k+1)}$ has two special properties not shared with the family $M_{k,\theta}$. The first is an assumption of additional symmetry not possible for $\theta \neq \pi/(k+1)$: namely, the existence of $k+1$ vertical planes of symmetry, as was the case for $M_k = M_{k,0}$ (see Figure 14).

Reflection in these planes descends to Σ, and then to the torus T as a single orientation-reversing involution. This involution of T must correspond to reflection in a line that itself is invariant under reflection in $\operatorname{Im} u = 0, \frac{1}{2}$; such a line must be vertical. The fixed point set of this reflection contains the set $\{e_1, e_2, v_1, v_2\}$, and so must consist of a pair of vertical lines invariant under 180° rotation around $\mathcal{D}$. Thus the involution is reflection in the lines $\operatorname{Re} u = 0, \frac{1}{2}\tau$, and the set $\{e_1, e_2, v_1, v_2\}$ consists of the half-period points of T. Without loss of generality, we may assume that e_1 lies at the center point of T; symmetry with respect to $\mathcal{D}$ dictates the placement of e_2, v_1 and v_2. All this is summarized in Figure 13.

The second distinctive property of $M_{k,\pi/(k+1)}$ is that g^{k+1} is well-defined on T. (This is the case even without the assumption of reflective symmetry.) On $M_{k,\pi/(k+1)}$, and hence on the quotient Σ, the Gauss map is vertical at the points over

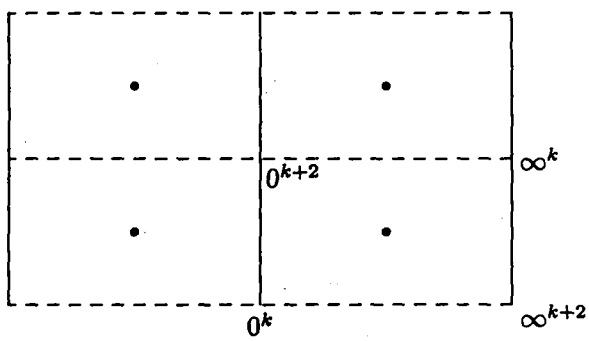

FIGURE 15. The pole structure of g^{k+1}.

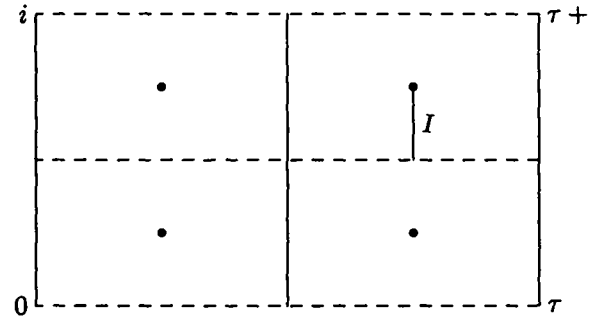

FIGURE 16. The path I in the domain.

e_i and v_i, having branching order k at the points over v_1, v_2 and $k+2$ at the points over e_1, e_2. The $(k+1)$-fold covering $\Sigma \to T$ is branched over these points, so g^{k+1} has these same branching orders at the points e_1, e_2, v_1, v_2. If we orient the surface so that $g^{k+1}(e_1) = 0$, we arrive at the zero-pole structure of g^{k+1} indicated in Figure 15; we already know that there are no other zeros or poles. Thus g^{k+1} is determined up to a nonzero multiplicative constant.

Because g must be unitary at the fixed points of the normal rotation on Σ, g^{k+1} is unitary on $\mathcal{D} \subset T$. Multiplication of g by a unitary number $e^{i\varphi}$ is equivalent to a rotation by φ around the vertical axis, which is irrelevant to the geometry of the surface. This means that the Gauss map of $M_{k,\pi/(k+1)}$ will be completely determined if we insist that g^{k+1} be unitary on $\mathcal{D}$.

6.2. The Period Problem

From Section 6.1, we now know that the only freedom we have in the Weierstrass data is the conformal type of the rectangular torus. We will now show that there is only one period to worry about; the assumed symmetries of $M_{k,\pi/(k+1)}$ make the period problem one-dimensional.

The horizontal lines of Σ over $\operatorname{Im} u = 0$ and the horizontal lines over $\operatorname{Im} u = \frac{1}{2}$ lie directly over one another. The horizontal axis of normal rotation bisects the angle between the successive lines on the surface above and below it; when $\theta = \pi/(k+1)$, the points on the surface above $\mathcal{D} \subset T$ (that is, the points where the horizontal normal-rotation axes meet the surface) necessarily lie in the same vertical plane as the lines on the surface, which are aligned vertically as they were on $M_k = M_{k,0}$.

We can express this in terms of the Weierstrass representation as follows. First we rotate the surface around the vertical axis so that one of the horizontal lines above $\operatorname{Im} u = 0$ is parallel to the x_2-axis; this is equivalent to requiring g to be real along this line. Then we must have

$$\operatorname{Re} \int_I (g^{-1} - g)\, dh = \operatorname{Re} \int_I (g^{-1} - g) i\, du = 0, \quad (6.2.1)$$

where I is the vertical segment beginning on $\operatorname{Im} u = \frac{1}{2}$ and ending at $\frac{3}{4}\tau + \frac{3}{4}i \in \mathcal{D}$ (Figure 16). This condition guarantees that the horizontal symmetry normal through the endpoint of I lies in the $x_1 = 0$ plane; the built-in symmetry will ensure that this is true everywhere. The reflective symmetries also ensure that there is no period on a horizontal generator of the torus; in fact the existence of normal-rotational symmetries already implies this, as was observed in Section 4.6.

We have one real period condition (6.2.1) and one free parameter, τ, describing the rectangular torus; one might expect a solution. However, we will prove in Section 6.4 that there is no solution.

6.3. Expression of g in Terms of Jacobi-Type Elliptic Functions

To show that (6.2.1) is not solvable for any rectangle, we will utilize some of the basic degree-two elliptic functions introduced in [Karcher 1988] or

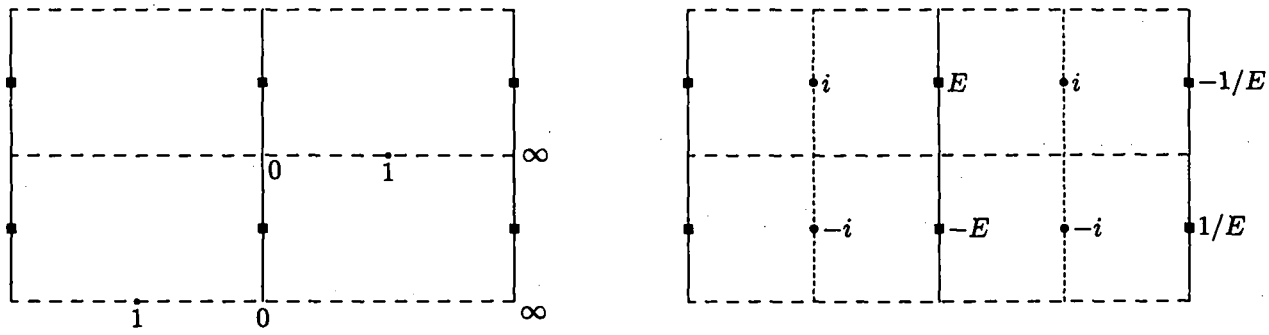

FIGURE 17. The translated half-period lattice $\mathcal{E}$ is indicated by solid squares. The quotient of the torus by a 180° rotation r_E about $\mathcal{E}$ is a sphere T/r_E. Assigning three complex values (left) to points on this sphere determines $\mathfrak{I}_E$. Values of $\mathfrak{I}_E$ are real along horizontal dashed lines, imaginary along vertical solid lines, unitary on the vertical dotted lines. Branch values $\pm E^{\pm 1} \in i\mathbf{R}$ are also indicated (right).

[Hoffman et al. 1994, § 3]. The functions we will use are called $\mathfrak{I}_E$ and $\mathfrak{I}_F$. We will construct $\mathfrak{I}_E$ directly, and then express $\mathfrak{I}_F$ in terms of $\mathfrak{I}_E$.

We construct $\mathfrak{I}_E$ as follows. Translate the half-period lattice by $\frac{1}{4}i$, producing the lattice points $\mathcal{E}$ indicated by small squares in Figure 17. The 180° rotation r_E about these points is an involution of the torus T; the quotient T/r_E is a sphere, twice covered by T. Once we identify this sphere with $\mathbf{C} \cup \{\infty\}$, we have a degree-two elliptic function, branched at the points of $\mathcal{E}$.

We completely determine this identification by specifying the values of three points of the sphere (Figure 17). We do this with the following in mind: we want $\mathfrak{I}_E$ to have simple zeros and poles on the half-period lattice and, in particular, a zero at the center; and we want $\mathfrak{I}_E$ to be real on the horizontal bisector of T. The first requirement plus the fact that $\mathfrak{I}_E \circ r_E = \mathfrak{I}_E$ force the placement of the zeros and poles. We choose to meet the second by specifying 1 as the complex value associated to the points on the sphere T/r_E, as indicated in Figure 17. Now $\mathfrak{I}_E$ is completely determined.

Observe that reflection ρ in the horizontal lines $\operatorname{Im} u = 0, \frac{1}{2}$ is an orientation-reversing involution with the property that it commutes with the 180° rotation of T about $\mathcal{E}$. Hence ρ passes to the quotient $T/r_E = S^2$, and there also it is an orientation-reversing involution. Its fixed-point set is a circle through 0, 1 and ∞, that is, the real line. Hence $\mathfrak{I}_E$ is real on the fixed-point set of ρ, the horizontal lines $\operatorname{Im} u = 0, \frac{1}{2}$. A similar reasoning shows that $\mathfrak{I}_E$ is unitary on $\operatorname{Re} u = \frac{1}{4}, \frac{3}{4}$, and that $\mathfrak{I}_E$ is imaginary on $\operatorname{Im} u = \frac{1}{4}, \frac{3}{4}$. It then follows that $\mathfrak{I}_E = \pm i$ on the points of $\mathcal{D}$. Correct choice of orientation dictates the value $+i$, as in Figure 17. In particular, $\mathfrak{I}_E$ has imaginary values at its branch points $\mathcal{E}$.

We denote by $\pm E^{\pm 1} \in i\mathbf{R}$ the values of $\mathfrak{I}_E$ on $\mathcal{E}$. The value of E is determined by the parameter τ that specifies the rectangular lattice.

In order to express g^{k+1} using $\mathfrak{I}_E$, we need one other elliptic function that we will produce from $\mathfrak{I}_E$ by a translation and a Möbius transformation. The translation is $\mathfrak{t}(u) = u + \frac{1}{4}(\tau - i)$, which moves $\mathcal{E}$ to the lattice $\mathcal{F}$ marked by solid squares in Figure 18.

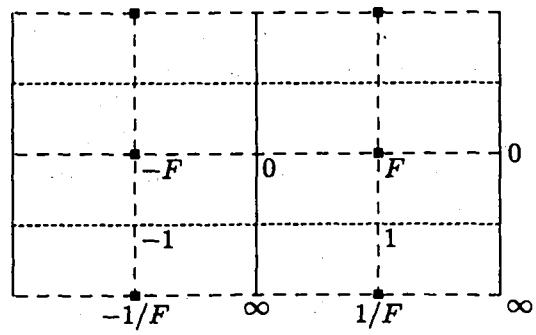

FIGURE 18. The function $\mathfrak{I}_F$. Values are imaginary along vertical solid lines, real along dashed lines, and unitary on horizontal dotted lines.

The Möbius transformation is

$$z \mapsto \frac{-z+i}{z+i},$$

which takes 0 to 1, ∞ to -1, i to 0, the real axis to the unit circle, the imaginary axis to the real axis, and the unit circle to the imaginary axis. We define $\mathfrak{I}_F$ by

$$\mathfrak{I}_F = \frac{-\mathfrak{I}_E \circ \mathbf{t} + i}{\mathfrak{I}_E \circ \mathbf{t} + i}.$$

The branch values of $\mathfrak{I}_F$, which we denote by $\pm F^{\pm 1}$, are real.

We are now in a position to express g^{k+1} in terms of $\mathfrak{I}_E$ and $\mathfrak{I}_F$. We simply note that $\mathfrak{I}_E^{k+1}\mathfrak{I}_F$ has the same zeros and poles, to the same order, as g^{k+1}, and is unitary on $\mathcal{D}$. By the results of Section 6.1, we have $g^{k+1} = \mathfrak{I}_E^{k+1}\mathfrak{I}_F$ and

$$g = \mathfrak{I}_E \sqrt[k+1]{\mathfrak{I}_F}. \tag{6.3.1}$$

Here g lives on Σ, which is a $(k+1)$-fold cover of T. We may, however, compute locally and consider points of T as corresponding to an appropriate lifting to Σ.

6.4. The Obstruction to the Solution of the Period Problem

Because $\mathfrak{I}_F$ has no zeros on the interval I of Figure 16 and is equal to 1 at one endpoint of I, its value F at the other endpoint is positive. Choose the branch of $\sqrt[k+1]{\mathfrak{I}_F}$ that is real and positive at this point. Then this branch is real from v_1 to e_1. The function $\mathfrak{I}_E$ is real on this line and it follows from (6.3.1) that g is real along this line. We already know that its image is a horizontal line, and, since g is real along it, it must be parallel to the x_2-axis. Now we may use the period condition (6.2.1). On I we have

$$dh = i\,du = -dt,$$
$$g = \sqrt[k+1]{\mathfrak{I}_F}\,\mathfrak{I}_E = f(t)e^{i\varphi(t)},$$

where $f(t)$ is the positive $(k+1)$-st root of $\mathfrak{I}_F$ at $I(t) := \frac{3}{4}\tau + it$, for $\frac{1}{2} \le t \le \frac{3}{4}$, and $e^{i\varphi(t)}$ is the value of $\mathfrak{I}_E$ at $I(t)$. We know that $\varphi(t)$ is monotonic and that $\varphi(\frac{1}{2}) = 0$ and $\varphi(\frac{3}{4}) = \pi/2$. Because $\mathfrak{I}_F$ has no branch points in $\mathring{I}$, the function $\mathfrak{I}_F$ is not equal to 1 anywhere on $\mathring{I}$ (and, for that matter, $F \neq 1$). Hence the expression

$$\begin{aligned}\operatorname{Re}(g^{-1} - g) &= \operatorname{Re}((f^{-1} - f)\cos\varphi - i(f^{-1} + f)\sin\varphi) \\ &= (f^{-1} - f)\cos\varphi\end{aligned}$$

never changes sign on I, and is nonzero on $\mathring{I}$. It follows that

$$\begin{aligned}\operatorname{Re}\int_I (g^{-1} - g)\,dh \\ = -\int_{\frac{1}{2}}^{\frac{3}{4}} \operatorname{Re}\left(g^{-1}(\tfrac{3}{4}\tau + it) - g(\tfrac{3}{4}\tau + it)\right)\,dt\end{aligned}$$

can never be zero, no matter what the value of τ. Hence there is no rectangular torus for which the period problem (6.2.1) can be solved; the surface $M_{k,\pi/(k+1)}$ does not exist with reflective symmetry.

ACKNOWLEDGEMENTS

We are grateful to Jim Hoffman of GANG, at the University of Massachusetts, whose graphics software was critical in the work described in this paper and who helped produce the images appearing in the paper.

REFERENCES

[Callahan et al. 1988] M. Callahan, D. Hoffman, and J. Hoffman, "Computer graphics tools for the study of minimal surfaces", *Communications of the ACM* **31** (1988), 648–661.

[Callahan et al. 1989] M. Callahan, D. Hoffman, and W. H. Meeks III, "Embedded minimal surfaces with an infinite number of ends", *Inventiones Math.* **96** (1989), 459–505.

[Callahan et al. 1990] M. Callahan, D. Hoffman, and W. H. Meeks III, "The structure of singly-periodic minimal surfaces", *Inventiones Math.* **99** (1990), 455–481.

[do Carmo 1976] M. do Carmo, *Differential Geometry of Curves and Surfaces*, Prentice Hall, New Jersey, 1976.

[Hoffman 1987a] D. Hoffman, "The computer-aided discovery of new embedded minimal surfaces", *Mathematical Intelligencer* **9**(3) (1987), 8–21.

[Hoffman 1987b] D. Hoffman, "The construction of families of embedded minimal surfaces", pp. 25–36 in *Variational Methods for Free Surface Interfaces* (edited by P. Concus and R. Finn), Springer-Verlag, New York, 1987.

[Hoffman 1993] J. T. Hoffman, MESH *manual*, preprint 35 (series 2), GANG, Univ. of Massachusetts at Amherst. See "Software Availability" below.

[Hoffman and Karcher] D. Hoffman and H. Karcher, "Complete embedded minimal surfaces of finite total curvature", in preparation.

[Hoffman et al.] D. Hoffman, H. Karcher, and W. H. Meeks III, "One-parameter families of embedded complete minimal surfaces of finite topology", in preparation.

[Hoffman et al. 1994] D. Hoffman, H. Karcher, and F. Wei, "The genus one helicoid and the minimal surfaces that led to its discovery", to appear in *Global Analysis and Modern Mathematics*, Publish or Perish, 1994.

[Hoffman et al. 1993] D. Hoffman, H. Karcher, and F. Wei, "Adding handles to the helicoid", *Bull. Amer. Math. Soc.* **29** (1993), 77–84.

[Hoffman and Meeks 1985a] D. Hoffman and W. H. Meeks III, "A complete embedded minimal surface in $\mathbf{R}^3$ with genus one and three ends", *J. Diff. Geom.* **21** (1985), 109–127.

[Hoffman and Meeks 1985b] D. Hoffman and W. H. Meeks III, "Complete embedded minimal surfaces of finite total curvature", *Bull. Amer. Math. Soc.* **12** (1985), 134–136.

[Hoffman and Meeks 1987] D. Hoffman and W. H. Meeks III, "Properties of properly embedded minimal surfaces of finite total curvature", *Bull. Amer. Math. Soc.* **17** (1987), 296–300.

[Hoffman and Meeks 1990] D. Hoffman and W. H. Meeks III, "Minimal surfaces based on the catenoid", *Amer. Math. Monthly* **97** (1990), 702–730.

[Hoffman and Wohlgemuth] D. Hoffman and M. Wohlgemuth, "New embedded periodic minimal surfaces of Riemann-type", in preparation.

[Karcher 1988] H. Karcher, "Embedded minimal surfaces derived from Scherk's examples", *Manuscripta Math.* **62** (1988), 83–114.

[Karcher 1989a] H. Karcher, "Construction of minimal surfaces", pp. 1–96 in *Surveys in Geometry*, University of Tokyo, 1989, and Lecture Notes No. 12, Sonderforschungsbereich 256, Bonn, 1989.

[Karcher 1989b] H. Karcher, "The triply periodic minimal surfaces of Alan Schoen and their constant mean curvature companions", *Manuscripta Math.* **64** (1989), 291–357.

[Lawson 1971] H. B. Lawson, Jr., *Lectures on Minimal Submanifolds*, Publish or Perish, Berkeley, 1971.

[Meeks and Rosenberg 1994] W. H. Meeks III and H. Rosenberg, "The geometry of periodic minimal surfaces", to appear in *Comm. Math. Helvetici.*

[Osserman 1986] R. Osserman, *A Survey of Minimal Surfaces* (2nd ed.), Dover, New York, 1986.

[Press et al. 1986] W. Press, B. Flannery, S. Teukolsky, and W. Vetterling, *Numerical Recipes*, Cambridge University Press, Cambridge, 1986.

[Schoen 1983] R. Schoen, "Uniqueness, symmetry, and embeddedness of minimal surfaces", *J. Diff. Geom.* **18** (1983), 791–809.

[Wei] F. Wei, "Singly periodic, embedded minimal surfaces of even genus", in preparation.

[Wei 1991] F. Wei, "The existence and topology of properly embedded minimal surfaces in $\mathbf{R}^3$", Ph.D. thesis, University of Massachusetts at Amherst, 1991.

[Wei 1992] F. Wei, "Some existence and uniqueness theorems for doubly periodic minimal surfaces", *Invent. Math.* **109** (1992), 113–136.

[Wohlgemuth 1991] M. Wohlgemuth, "Higher genus minimal surfaces by growing handles out of a catenoid", *Manuscripta Math.* **70** (1991), 397–428.

SOFTWARE AVAILABILITY

The MESH program is available by ftp from `ftp.gang.umass.edu`, in directory `pub/mesh`.

A Quicktime animation of the evolution of the surfaces described here is available on the same host, in directory `user/oliver/qt`. For more details, contact David Oliver at `oliver@gang.umass.edu`.

Michael Callahan, Mathematical Institute, Oxford University, Oxford OX1 3JP, England (callahan@maths.ox.ac.uk)

David Hoffman, Department of Mathematics, University of Massachusetts, Amherst, MA 01003, USA (david@smectos.gang.umass.edu)

Hermann Karcher, Mathematisches Institut, Universität Bonn, D-53115 Bonn, Germany

Received August 25, 1993; accepted October 15